



**HAL**  
open science

## The potential of flax shives as reinforcements for injection moulded polypropylene composites

Lucile Nuez, Johnny Beaugrand, Darshil Shah, Claire Mayer-Laigle, Alain Bourmaud, Pierre D'arras, Christophe Baley

► **To cite this version:**

Lucile Nuez, Johnny Beaugrand, Darshil Shah, Claire Mayer-Laigle, Alain Bourmaud, et al.. The potential of flax shives as reinforcements for injection moulded polypropylene composites. *Industrial Crops and Products*, 2020, 148, pp.112324. 10.1016/j.indcrop.2020.112324 . hal-02544204

**HAL Id: hal-02544204**

**<https://hal.inrae.fr/hal-02544204v1>**

Submitted on 22 Aug 2022

**HAL** is a multi-disciplinary open access archive for the deposit and dissemination of scientific research documents, whether they are published or not. The documents may come from teaching and research institutions in France or abroad, or from public or private research centers.

L'archive ouverte pluridisciplinaire **HAL**, est destinée au dépôt et à la diffusion de documents scientifiques de niveau recherche, publiés ou non, émanant des établissements d'enseignement et de recherche français ou étrangers, des laboratoires publics ou privés.



Distributed under a Creative Commons Attribution - NonCommercial 4.0 International License

1 **The potential of flax shives as reinforcements for injection moulded polypropylene composites**

2 Lucile Nuez<sup>1,2\*</sup>, Johnny Beaugrand<sup>3</sup>, Darshil Shah<sup>4</sup>, Claire Mayer-Laigle<sup>5</sup>, Alain Bourmaud<sup>1</sup>, Pierre  
3 D'Arras<sup>2</sup> and Christophe Baley<sup>1</sup>

4 1 : Université de Bretagne-Sud, IRDL, CNRS UMR 6027, BP 92116, 56321 Lorient Cedex, France

5 2: Van Robaeys Frères, 83 Rue Saint-Michel, 59122 Killen, France

6 3: Biopolymères Interactions Assemblages (BIA), INRAE, Rue de la Géraudière, F-44316 Nantes,  
7 France

8 4: Centre for Natural Material Innovation, Department of Architecture, University of Cambridge,  
9 Cambridge CB2 1PX, United Kingdom

10 5: UMR 1208 IATE, Cirad, INRA, Montpellier SupAgro, Université de Montpellier, 2 place Pierre Viala,  
11 4060 Montpellier Cedex 02, France

12

13 \* Corresponding author: *e-mail address* alain.bourmaud@univ-ubs.fr

14 Tel.: +33-2-97-87-45-18; Fax: +33-2-97-87-45-88

15

16 **Abstract**

17 Flax shives (FS) represent approximately 50% in weight of dry flax stems, making it the main by-  
18 product of the flax scutching industry. Being an available and low-added value lignocellulosic  
19 resource, flax shives are an interesting candidate for thermoplastic composite reinforcement. In this  
20 study, raw flax shives were fragmented by knife milling using two grids of 500 and 250  $\mu\text{m}$   
21 respectively, while a third batch, with a targeted particle size below 50  $\mu\text{m}$ , was obtained by an attrition  
22 beads mill. The fragmentation methods used do not modify the biochemical composition of FS but do  
23 reduce their crystallinity due to both crystalline cellulose allomorph conversion and amorphization. The  
24 poly-(propylene) and 4%-wt maleic anhydride modified poly-(propylene) injection moulded composites  
25 produced with these reinforcing materials have a maximum tensile strength that evolves linearly with  
26 particle aspect ratio after processing. The tensile Young's modulus of the composites reinforced by  
27 coarser particles is  $3268 \pm 240$  MPa, which is almost 90% that obtained for a reference 1 mm flax fibre  
28 reinforced composite. Furthermore, a basic micromechanical model was applied highlighting the  
29 reinforcing capacity of cell wall-like small tubular structures (e.g. flax shives). This study underlines the  
30 reinforcing potential of low-value by-product flax shives for value-added composite applications.

31

32 **Keywords**

33 Flax shives, injection moulding, morphology, mechanical properties, X-ray diffraction

34

35 **1. Introduction**

36 The development of the biocomposite industry in the past few decades due to ecological concerns has  
37 notably contributed to a growing interest in the plastic composite reinforcing potential of various  
38 agricultural by-products such as woody hemp core [1], sugarcane bagasse, sunflower and corn stalk  
39 [2], rice hull, corn cob and walnut shell flour [3]. Driven by eco-responsibility reasons such as the  
40 reduction of synthetic petrochemical consumption, the use of agricultural by-products represents a  
41 potential economically viable solution for local economy waste management, so long as transportation  
42 and transformation costs are limited. As flax cultivation areas are increasing (+8% in France from 2017  
43 to 2018), so are the quantities of agricultural by-products from the flax scutching industry. Flax shives  
44 might then even be an alternative to the widely used wood flour in wood plastic composites (WPC),  
45 and their addition to wood flour could contribute to reducing the cost of such materials alongside  
46 recycling waste. Indeed, flax is an annual plant which temporarily stores carbon dioxide during growth  
47 [4, 5]. In the case of France, the flax cultivation areas are geographically concentrated along the  
48 English canal (from Normandie to the North), and this is a major advantage for material transportation  
49 from the production site to the end-use factory.

50 When cultivated for its fibre, flax stems are grown to be approximately one metre in height with a  
51 diameter of up to 3 mm [6]. When mature, stems are harvested, undergo a retting step followed by a  
52 scutching process in order to extract the high added-value bast fibres. The retted stems are crushed  
53 by successive fluted rollers, and then beaten from bottom up in order to separate the fibres from the  
54 rest of the stem constituents, mainly from flax shives (FS) which are a cause of quality defects in the  
55 fibre transformation processes. FS represent around 50% in weight of retted flax stems [7], which  
56 makes them the main by-product of the flax fibre production process. Traditionally used for soil  
57 amendment, animal bedding or particle boards for building insulation [8], FS have also been studied  
58 as a resource for various innovative applications including activated carbon [9], 3D printed lightweight  
59 concrete [10], and bio-fuel production [11]. FS have a low added value, a low density and, above all,

60 are a widely available resource which flax scutching companies wish to broaden the areas of  
61 application of, and this makes them a genuine potential reinforcing material in bio-composites.

62 Flax shives, also referred to as woody core, have a highly lignified structure made of the inner tissues  
63 of the stem, namely the pith, the xylem and the phloem, the last two having a role in the conduction of  
64 raw and elaborated sap, respectively. Studying the transverse section of flax stems, Goudenhooff et  
65 al. measured the tissue content to be between 70 and 85% depending on the flax variety, and the  
66 xylem represents about 75% of the total tissue content [6, 12]. They also found, by stem flexural  
67 bending tests, that the woody core has a structural role and accounts for up to 30% of dry flax stem  
68 bending stiffness due to architectural differences and lower density.

69 The composition of flax shives is approximately 25% lignin, 50% cellulose, and 20% hemicellulose [3,  
70 13], but this varies depending on the analytical method, plant maturity and even location of FS in the  
71 stem. Day et al. [14] found that lignin content ranges from 24% to 32% in the inner tissues depending  
72 on maturity and location in the stem, against only 1.5% to 4.2% in the dry cell wall resides in the outer  
73 tissues (specifically fibre bundles imbedded in the parenchyma, the cortical parenchyma, and the  
74 phloem).

75 Raw bulk flax shives demonstrate a considerable particle size distribution, with particles as long as  
76 40 mm [10] and thus can be difficult to use as such for efficient polymer reinforcements. Consequently,  
77 a mechanical size reduction step such as comminution by grinding is useful in controlling particle  
78 granulometry, size distribution and aspect ratio (ratio of length over particle width or fibre diameter).

79 Knife milling can be used as a first reduction step (from the meter scale to that of the centimetre) of  
80 forages or stems [15]. In this grinder, particles are fed continuously and the comminution is mainly  
81 achieved by shear mechanisms. The size of the ground particles is determined by the size of the hole  
82 of the sieving grid (from a few millimetres to hundreds of micrometres) at the output of the milling  
83 chamber. On the other hand, small particles (10-500  $\mu\text{m}$ ) can be obtained by media milling, which  
84 consists of breaking down batches of particles by compression and attrition mechanisms thanks to a  
85 milling media (ball or beads) put in motion by a rotor, a vibrating or rotary tank. This technique allows  
86 to reach very fine particles but the total energy consumption is higher due to long residence time  
87 required to obtain such fine granulometries [16]. In addition it has also been proven that such  
88 technologies reduce the crystallinity of plant cell wall cellulose [17, 18].

89 In composites, the bonding efficiency will determine the quality of stress transfer between  
90 reinforcement and matrix. When plant fibres are embedded in a polymer matrix, they generally  
91 increase its stiffness and reduce tensile deformation. An optimal fibre volume fraction has been  
92 observed in injection moulded PP composites after which tensile strength decreases; this is around  
93 33%-vol specifically in the case of flax-PP composites [19, 20, 21]. The impact of reinforcing fibres on  
94 composite mechanical properties depends in particular on fibre orientation which in the case of short  
95 fibre reinforced injection moulded composites depends on the severity of the skin-core effect.  
96 Morphology and structure of plant reinforcement also plays a major role in fibre orientation [22]. Fibre  
97 length, tendency of packing, viscosity, process parameters, all influence the thickness of the skin layer  
98 which contains the most fibres parallel to the melt flow direction and accounts for higher mechanical  
99 properties [22, 23, 24]. The higher the fibre aspect ratio, the higher the mechanical properties. Stark et  
100 al. [25] compared the role of wood flour and wood fibre having approximate aspect ratios of 4 and 16  
101 respectively. When incorporated with MAPP in injection moulded composites, they found that tensile  
102 strength of the latter increased between 30 and 60% depending on the amount of wood fibre  
103 compared to wood flour composites. While the aspect ratio of flax fibres will depend on fibre fineness  
104 and processing [26, 27], that of flax shives will depend highly on the mode of comminution.  
105 The aim of this study is to evaluate the reinforcing potential of flax shives, a by-product of flax fibre  
106 crop. In order to situate the mechanical properties of FS injection moulded PP composites, a panel of  
107 different plant cell walls were tested for comparative purposes. This analytical investigation is based  
108 on a two-level strategy. First, the FS structure was examined by particle size analysis following two  
109 methods of comminution (knife or attrition beads milling). An ultrastructural study of these fragmented  
110 FS was carried out by X-ray diffraction analysis. Additionally, the constitutive polymers of FS were  
111 characterised by biochemical analysis. Second, at the scale of the composites, mechanical properties  
112 of injection moulded composites were measured, specifically interrogating the impact of FS particle  
113 size and filler volume fraction (from 0% to 31%). Finally, a theoretical approach to determine FS critical  
114 length was discussed with the help of a simplified mechanical model, to understand the reinforcing  
115 potential of small and hollow cell wall structures such as shives.  
116

## 117 2. Experimental

### 118 2.1. Matrix polymer

119 The matrix used in this study is polypropylene, chosen because it is a commodity polymer widely  
120 used in the automotive industry. PPC 10642 was supplied by Total Petrochemicals (France) with a  
121 MFI of 44 g/ 10 min at 230°C and 2.16 kg, and a polymer density of 0.94. Because plant cell walls  
122 have an important polysaccharide content giving them a hydrophilic nature, maleic anhydride modified  
123 polypropylene (MAPP) was added to the formulation as compatibilizer for its amphiphilic nature  
124 enabling bonding with both the hydroxyl groups of the filler and the hydrophobic polymer matrix [28].  
125 MAPP (Orevac CA 100) was supplied by Arkema (France) and has an MFI of 10 g/10 min (at 190 °C  
126 and 0.325 kg), 4% of MAPP were added to the formulation during the compounding process as it  
127 represents a good compromise between bonding improvement and cost of polymer [29].

128

### 129 2.2. Reinforcing materials

130 The flax shives used in this study were provided in bulk by the flax scutching company Van Robaeys  
131 Frères (France) following the scutching of the 2018 flax harvest year, before being milled with a  
132 laboratory scale rotating cutting mill (Retsch Mühle, Germany). The mesh size of the grids used were  
133 either 500 µm or 250 µm. To obtain finer powder, the powder ground with the knife mill (250 µm-  
134 grids) have been submitted to an additional milling step in an attrition beads mill, as the previous  
135 technique is not adapted to obtain such fine granulometries [30]. The equipment employed is a  
136 laboratory prototype, composed of a milling chamber of 3 L in which 175 g of the powder to grind and  
137 7.5 kg of small steel beads (6 mm) are put in motion by a rotor at 300 rpm. The milling time (100 min)  
138 was determined so that at least 90% of micronized particles have a diameter below 50 µm.

139 The flax fibre (*Linum usitatissimum* L.) used is from the Alizée variety, which was harvested in 2017 in  
140 Normandy (France), and was scutched and hackled before being cut to 1 mm in length and supplied  
141 as such by Depestele (France). In the rest of this study, the term “fibre” will designate both elementary  
142 fibres and flax fibre bundles as both are present in the studied batch; otherwise differentiation will be  
143 made by specifying “elementary fibres” or “bundles”.

144 An additional sample of wood flour was studied for comparative purposes as it is commonly used in  
145 the wood plastic composites industry. This sample is composed of a mixture of untreated *pinus*  
146 *pinaster* and *picea sitchensis* wood chips originating from sawmill residues, therefore precise history

147 and composition is unknown. They have further been dried, fragmented by hammer milling with a 1  
148 mm grid and sieved. The fraction under the 800  $\mu\text{m}$  sieving mesh size was studied here. All reinforcing  
149 materials and their corresponding abbreviations as they will be used throughout the article are given  
150 Table 1.

151

### 152 *2.3. Particle size analysis*

153 Particle morphology was studied by a dynamic image analysis device, QICPIC (SympaTec GmbH,  
154 Germany). Two shape factors were determined (i) the particle length, defined as the shortest path  
155 between the most distant end points of the particles after skeletonization, (ii) an aspect ratio (length  
156 over diameter). The aim was to understand the effects of comminution on the granulometry of FS.  
157 Both the materials samples before and after extrusion and injection moulding (see section 2.6) were  
158 investigated. For the latter, samples were obtained from composites after dissolving the PP matrix with  
159 o-xylene at 150°C during 3 days by reflux. The extracted particles were then thoroughly washed with  
160 boiling xylene followed by acetone and left to dry overnight in a 60°C oven. All samples were oven  
161 dried at 60°C overnight before measurement in order to limit analysis bias caused by initial water  
162 content. Two protocols have been adapted for the particle morphometric description by the QICPIC.  
163 For the raw particles (flax shives and flax fibres), the most appropriate way was to disperse those  
164 samples with a vibrating chute VIBRI unit combined with a dry dispersion unit GRADIS, because of  
165 their important particle size and easy scattering. All the others samples micronized or extracted from  
166 composites were more appropriately analysed with a liquid dispersion unit, MIXCEL. Indeed, these  
167 batches displayed a tendency to particle aggregation so they were first dispersed in ethanol. To obtain  
168 accurate data in the morphological measurements, the QICPIC lenses (from M9 to M5) have been  
169 adapted to the size of each sample. The selection of the appropriate lens is based on initial visual  
170 coarseness of sample and supplier specifications. As we assume that the particle size variation  
171 remains weak before and after processing, the same lens was used in this case in order to obtain data  
172 in the same range. The number of analysed particles varied between 20,000 and 10 million depending  
173 on samples, measurements were made in triplicates to ensure reproducibility of the results. PAQXOS  
174 software (SympaTec GmbH, Germany) was used to calculate particle length and aspect ratio in real  
175 time.

176

177 *2.4. Biochemical composition*

178 The monosaccharide content of the sample lots (Table 1) were assessed by wet chemical analysis,  
179 aside from the extracted ones after extrusion-injection because of arguable extraction bias due to the  
180 o-xylem solvent used. Before hydrolysis, the large size of the R-FS, FF and WF particles requires a  
181 first step of homogenization done by cryogrinding (SPEX 6700 freezer Mill) of approximately 1g of  
182 materials. The whole panel of powdered samples (approx. 5 mg per assay) were then hydrolysed in 12  
183 M H<sub>2</sub>SO<sub>4</sub> (Sigma Aldrich) for 2 h at 25°C (heat plate) followed by additional hydrolysis of 2 h at 100°C  
184 with 1.5 M H<sub>2</sub>SO<sub>4</sub> in presence of inositol as internal standard. Galacturonic Acid (GalA) and  
185 Glucuronic Acid (GlcA) was determined by an automated m-hydroxybiphenyl method [31] and merged  
186 as Uronic acid (UrAc), whereas individual neutral monosaccharides (arabinose, rhamnose, fucose,  
187 glucose, xylose, galactose and mannose) were analysed as their alditol acetate derivatives [32] by  
188 gas-liquid chromatography (Perkin Elmer, Clarus 580, Shelton, CT, USA) equipped with an DB 225  
189 capillary column (J&W Scientific, Folsom, CA, USA) at 205°C, with H<sub>2</sub> as the carrier gas. Standards  
190 of carbohydrate solutions with three known concentrations were used for calibration. Analyses were  
191 performed in three independent assays. The total monosaccharide content is the sum of each  
192 monosaccharide amount, and is expressed as the percentage of the dry matter mass.  
193 The lignin content was quantified in the panel of samples (Table 1) from the homogenised micronized  
194 particles. Lignin was quantified by colorimetric analysis following the acetyl bromide method [33] on  
195 mass weight samples of approx. 20 mg per assay. The chemicals were laboratory grade from Sigma  
196 Aldrich and the analyses were performed in at least three independent assays, with lignin expressed  
197 as the percentage of the dry matter mass.

198

199 *2.5. X-Ray Diffraction*

200 Wide-angle X-ray diffraction (XRD) measurements were performed in triplicates under ambient  
201 conditions on a Siemens D500 diffractometer CuK $\alpha$  radiation. Samples were loaded on a silicon wafer  
202 and scans were collected from  $2\theta = 10$  to  $30^\circ$  with step size of  $0.03^\circ$  at 2 s/step, at 30 kV and 20 mA.  
203 Crystallinity was calculated based on the method developed by Segal et. al using Eq. 1, where  $I_{tot}$  is  
204 the intensity at the primary peak for cellulose I (at  $2\theta \approx 22.5^\circ$ ) and  $I_{am}$  is the intensity from the  
205 amorphous portion evaluated as the minimum intensity (at  $2\theta \approx 18.5$ ) [34][35].

206 
$$C = \frac{I_{tot} - I_{am}}{I_{tot}} \times 100 \quad (\text{Eq. 1})$$

207

208 *2.6. Preparation of composites*

209 Before processing, the reinforcing materials and PP-MAPP matrix were oven dried at 60 °C for at least  
210 12 hours. They were then compounded with a single-screw extruder (Fairex, England) at 190 °C and  
211 an extrusion speed of 25 rpm. The length and diameter of the screw were 600 and 20 mm  
212 respectively, inducing an aspect ratio L/D of 30. After granulation and oven-drying in the same  
213 conditions, the material under-went a second extrusion step using a TSA (Italy) co-rotating twin-screw  
214 extruder with a screw diameter of 20 mm and L/D ratio of 40. A temperature profile going from 180°C  
215 to 190°C and a die temperature of 180° C were imposed with a screw rotation speed of 300 rpm. The  
216 material was once more granulated, oven-dried, and ISO 527-2 type 1B normalised specimens were  
217 obtained using an 80 Tons Battenfeld (Austria) injection moulding machine with a constant barrel and  
218 mould temperature set at 190°C and 30 °C, respectively.

219

220 *2.7. Mechanical Characterization*

221 The injection moulded T-bone specimens were submitted to tensile testing following the ISO 527  
222 standard on an MTS Synergie 1000RT machine with a controlled environment (temperature of 23°C  
223 and relative humidity of 48%). Tensile speed was of 1 mm/min and nominal gauge length was 25 mm.  
224 A 10 kN sensor was used to measure the applied force on the specimen, and an extensometer was  
225 used to measure deformation during the tests.

226

227 *2.8. Density measurements*

228 The density of raw FS-500 was measured by helium pycnometer measurements based on the method  
229 described by Le Gall et al. [36]. Measurements were made in 10 replicates and the average value of  
230 1.43 g/cm<sup>3</sup> was obtained. The rule-of-mixtures was then applied to calculate the volume fraction in the  
231 composites knowing the density of the PP-MAPP matrix as follows (Eq. 2):

232 
$$\rho_c = \rho_{fs}V_{fs} + \rho_m(1 - V_{fs}) \quad \text{Eq. 2}$$

233 With  $\rho_c$ ,  $\rho_{fs}$ , and  $\rho_m$  the density in g/cm<sup>3</sup> of the composite, the flax shives and the matrix respectively,  
234 and  $V_{fs}$  the volume fraction of the reinforcing flax shives, calculated knowing the mass fraction and  
235 density of the components.

236

### 237 *2.9. SEM Observations*

238 The raw reinforcing materials were observed using a Joel JSM 6460LV (France) scanning electron  
239 microscope (SEM) after comminution and prior to composite processing after being sputter coated  
240 with a thin layer of gold in an Edwards Sputter Coater. The fracture surface of specimen following  
241 tensile testing were also observed by SEM.

242

243

## 244 **3. Results and discussions**

### 245 *3.1 Characterization of the reinforcing materials*

#### 246 *3.1.1 Validation of the experimental procedure*

247 First, a comparison between the number and volume length distributions is proposed in order to  
248 determine a valuable method of particle size analysis using the dynamic analyser used (QICPIC).

249 Particle morphology analysis provides significantly different information depending on measurement  
250 parameters such as equipment used, image resolution, automatic or “by-hand” measurements,  
251 causing specific particle size populations to be potentially left out [36, 37, 38].

252 The length distributions given in number and volume are schematically displayed by box-plot diagrams  
253 in Figure 1. Because a unique average value does not give any information on distribution span,  
254 symmetry, skewness or extreme values, box plots are preferred. It is a simple visual tool adequate to  
255 use in statistical analysis to evaluate data (median, span...) without making any suppositions on its  
256 distribution, especially when it does not follow a normal or log-normal law. The 10<sup>th</sup> (first decile), 16<sup>th</sup>,  
257 50<sup>th</sup> (median), 84<sup>th</sup>, and 90<sup>th</sup> (last decile) percentiles of the cumulative distribution in length are shown  
258 respectively from bottom up.

259 The number distributions (Fig. 1a) emphasise the quantity of small particles present in each batch, as  
260 each particle is given the same “weight” regardless of size. On the contrary, in the volume distribution  
261 (Fig. 1b), a “weight” is attributed to each particle corresponding to the volume of the particle divided by  
262 the total volume of particles analysed. In this study, the particle volume is assimilated to a cylinder of

263 which the length and diameter are those measured for each particle. Therefore, in this distribution  
264 small particles are somewhat obscured as their weight is much lower than that of larger particles.  
265 Both the distribution in number and in volume are complementary for readers to have a cognitive  
266 understanding of a population of particles, however in the aim of materials reinforcement when dealing  
267 with natural fibre, the distribution in volume is most desirable compared to the distribution in number  
268 [40] as this parameter is most representative of the volume fraction of reinforcing material and its role  
269 in the mechanical support of the composite.

270 Note also that small particles are composed of only few pixels and the precision in the determination of  
271 the shape factors are lower than for larger particles like fibres composed of hundreds of pixels. By  
272 choosing an adequate lens for the device, it is possible to increase the number of pixels of an element  
273 thanks to a shorter length scale of the pixel size, but in this case, it becomes difficult to focus on larger  
274 particles. Thus, for powders exhibiting broadly scattered particle sizes, the limitations of the device do  
275 not allow to have a high resolution for both small and large particles at the same time. This point  
276 should be kept in mind when comparing the different particle size distributions.

277 Figure 1a reveals that 84% of raw flax shives (R-FS) are made up of particles less than 90  $\mu\text{m}$  long,  
278 whereas the volume distribution shows that 16% of particles are less than 3052  $\mu\text{m}$  long. Except for  
279 FS-50, all initial reinforcing materials have at least 80% of their number distribution which lays  
280 completely out of their volume distribution. Shives are obtained during the scutching of flax, which also  
281 produces up to 10%-wt of dust from the retted straws originating mainly from cultivation step in the  
282 fields. An unknown part is left in the shives and is found in the initial R-FS and will be present in all  
283 batches as it won't be affected by comminution. This proportion of particles smaller than 200  $\mu\text{m}$   
284 (which represents the particle length limit commonly admitted as defining fines [41]) is present in all  
285 studied reinforcing materials as the FS-500, FS-250 and FF median lengths in number are of 8 or 9  
286  $\mu\text{m}$  against 484  $\mu\text{m}$ , 455  $\mu\text{m}$ , and 976  $\mu\text{m}$  in volume respectively.

287 The sample length distributions in volume (Fig. 1b) shows the initial R-FS median length is reduced by  
288 10 when using the knife-milling step in the case of FS-500. The latter's median length is then  
289 comparable to that of the FS-250 sample at 455  $\mu\text{m}$ . The 84<sup>th</sup> percentiles of FS-500 and FS-250 are at  
290 1518  $\mu\text{m}$  and 1134  $\mu\text{m}$  respectively, which is respectively 3 and 4.5 times more important than the  
291 initial milling grid mesh size. This can be explained by the grids' pattern which has a grating effect on

292 R-FS. Furthermore, the 84<sup>th</sup> percentile of FS-50 is of 30  $\mu\text{m}$ , making the length of this sample  
293 complementary to that of the last two samples for this study.

294 The morphological study of particles can be carried out by image analysis after observation under  
295 optical microscope of a sufficiently significant population of particles. Automated laser measurements  
296 have the advantage to be less operator dependant. Le Moigne et al. [37] found that 'by hand'  
297 measurements induced a discrepancy and had a tendency to magnify fibre dimensions due to  
298 operator dependence compared to using a specific software for fibre detection (50% of the number  
299 weighted length of flax fibres measured by hand were more than twice the length of the same particles  
300 detected by the software). Dynamic image analysis is a time-efficient method to obtain a wide amount  
301 of particle morphology information such as shape descriptors and distributions in number, length,  
302 surface or volume [38]. In the rest of this study, analysis is carried out on the basis of volume  
303 distributions.

304

### 305 3.1.2 Morphological analysis of raw reinforcing materials

306 Figure 2 shows the particle length distribution in volume as well as the overall aspect of the reinforcing  
307 materials as observed with SEM images. Prior to comminution, R-FS presents a very wide fibre length  
308 distribution with a median of about 4850  $\mu\text{m}$  and a main mode at 6300  $\mu\text{m}$ , which is similar to the "by-  
309 hand" optical measurements by Evon et al. [42] of  $5800 \pm 4013$   $\mu\text{m}$  of average length. The reference  
310 flax fibres present a homogeneous fibre length with a unimodal distribution having a median of 976  $\mu\text{m}$   
311 coherent with the targeted fibre length of 1 mm. Wood flour exhibits a heterogeneous length  
312 distribution, with a visually important aspect ratio, and a median length of 440  $\mu\text{m}$ . Wood flour used in  
313 this study originates from saw milling waste and was used as-received without any further sieving.  
314 FS-500 and FS-250, both fragmented using a knife milling device and milling grids of 500  $\mu\text{m}$  and 250  
315  $\mu\text{m}$  respectively, show several distinct particle populations: fine particles having a mode at  
316 approximately 70  $\mu\text{m}$  for both samples, and coarser particles with a mode of 1450  $\mu\text{m}$  and 1000  $\mu\text{m}$ ,  
317 respectively. This similar behaviour can be explained by the comminution process for which raw FS  
318 are continually fed to the machine inducing an unknown residence time, causing certain particles to be  
319 more fragmented than others. In addition to this, we can assume that depending on the origin of FS  
320 (e.g. type of cell, position in the plant, plant maturity), the differences in cell wall rigidity (varying  
321 amount of lignification depending on the role of the cells in the plant) and specific mechanical strength

322 of initial R-FS will have an effect on the kinetics of fragmentation and disaggregation. Flax xylem  
323 compressive strength at break measured from 3-point bending tests carried out on peeled flax stems  
324 is approximately 60 MPa, which is a third of the strength of the whole stem [43]. **The mostly xylem**  
325 **origin of FS also explains why the fine particle population visible on the SEM images of both FS-500**  
326 **and FS-250 is absent in that of FF. Furthermore, contrasting initial processing steps may bring further**  
327 **insight on this phenomenon as flax fibres were hackled before being cut, which further removes**  
328 **residual cortical tissues from fibre bundles and therefore reduce the amount of fines in the sample.**

329 Figure 3 shows that the alveolar structure of FS from the plant's xylem is preserved after knife-milling  
330 providing a reinforcing material with hollow tubular sections corresponding to dry conduction vessels  
331 or supporting xylem cells. Indeed, in a knife mill, the compression mechanism remains weaker in  
332 comparison to shear mechanism and the type of mill is known to preserve the structure of the plant  
333 materials [44].

334 Furthermore, Figure 2 shows that particle length distribution of FS-50 is very narrow, with a first decile,  
335 a median, and a last decile of 9  $\mu\text{m}$ , 17  $\mu\text{m}$ , and 33  $\mu\text{m}$  respectively, accounting for a homogeneous  
336 particle fragmentation justified by the intensity of the 23-hour ball milling process. This panel of results  
337 exhibits the strong impact of the material preparation (cutting, knife milling, or ball milling) on particle  
338 morphology and structure.

339

### 340 3.1.3 Biochemical analysis

341 The monosaccharide and lignin content of the different samples are given Figure 4. Considering that  
342 glucose accounts for sample's content in cellulose, then flax fibres FF are made of 70% of cellulose on  
343 average (out of total dry matter content) compared to only 30% for flax shives FS and 42% for wood  
344 flour WF; and approximately 3% of lignin for FF, against 30% for WF and R-FS. The latter also contain  
345 about 16 times more xylan than FF which is in agreement with measurements carried out by Buranov  
346 et al. [30, 44]. The differences in biochemical composition can be explained by the contrasting **origins**  
347 **and** functions of cells in the flax stem. Due to their high mechanical role, flax fibres possess well  
348 developed secondary cell walls made up of cellulose microfibrils and can be considered as gelatinous  
349 fibres [46] with low lignification. In contrast, xylem cells have a role in the mechanical support of the  
350 plant and so have a secondary cell wall, but are responsible for raw sap conduction and therefore are

351 highly lignified from the base to the top of the plant [47], also highlighted by the progressive  
352 lignification of the xylem throughout plant growth [14].

353 Since the wood flour comes from fluctuant sawmill wastes, it is a blend of both soft and hardwood but  
354 the precise species origin is unknown, as well as its ratio. Therefore its biochemical composition was  
355 determined for information purposes and is in agreement with ranges found in the general  
356 literature [48].

357 Furthermore, the amount of cellulose, lignin and non-glucosidic monosaccharides does not  
358 significantly evolve in the FS samples following fragmentation, even in the case of intense milling in  
359 the attrition beds mill (FS-50). It is interesting to notice that contrary to ball milling known to cause a  
360 drop in cellulose content in wood or flax fibres, the intense milling employed here seems to preserve  
361 the total chemical composition of the powder. This is probably due to the shorter milling time (100 min  
362 compared to several hours in ball milling).

363

#### 364 3.1.4 XRD

365 The diffraction pattern of cellulose I (Fig. 1a) includes five major reflections for the crystalline phases  
366 at  $2\theta \approx 15^\circ$  ( $1\bar{1}0$  diffraction plane following the recommendations of French [49]),  $17^\circ$  ( $110$ ),  $21^\circ$  ( $102$ ),  
367  $22.5^\circ$  ( $200$ ) and  $34.5^\circ$  ( $004$ ), with the amorphous phase observed at  $2\theta \approx 18.5^\circ$  [35]. These reference  
368 peaks were used to analyse the XRD spectra of the various flax fibre samples (Fig. 5a).

369 All samples exhibit a primary peak at  $2\theta \approx 22.5^\circ$  corresponding to the crystalline 200 plane of cellulose  
370 I, however the peak is sharp and distinct for raw flax fibres, slightly broader for raw flax shives until  $2\theta$   
371  $\approx 12^\circ$  (belonging to cellulose II or III), supposing the presence of both cellulose I and cellulose II or III  
372 in raw flax shives. This peak gets broader (left-ward) with the severity of attrition beads milling (Fig.  
373 5a). In addition, raw flax fibres, and to an extent raw flax shives, exhibit the  $1\bar{1}0$  and  $110$  secondary  
374 peaks, while these peaks are less distinct for ball milled flax shives, and not discernible for FS-50. The  
375 noted qualitative observations and subsequent measurements (Fig. 5b) suggest a reduction in  
376 crystallinity (increase in level of disorder) of the shives with severity of ball milling, as was observed  
377 with after two hours of ball milling on crystalline cellulose [50]. Specifically, while raw flax fibres and  
378 shives have a crystallinity of 77.2% and 60.0%, respectively, the cellulose crystallinity reduces to  
379 41.7%, 38.8% and 28.9% for FS-500, FS-250 and FS-50, respectively. The latter is comparable to the  
380 crystallinity of wood flour (31.3%).

381 With increasing severity of ball milling, while no distinct shifts in diffraction peaks are observed, there  
382 is left-ward broadening of the  $2\theta \approx 22.5^\circ$  (belonging to 200 plane of crystalline cellulose I), and the  
383 presence of an additional and increasingly important peak at around  $2\theta \approx 12^\circ$  (which belongs to  
384 cellulose II or III) [51]. Notably, wood flour exhibits this prominent peak as well (Fig 5a). These indicate  
385 that cellulose II or III is becoming prominent with ball milling; typically, cellulose I irreversibly converts  
386 to cellulose II upon mercerisation or urea treatment [50, 51], and cellulose I can reversibly convert to  
387 cellulose III upon liquid ammonia treatment [52, 51]. Notably, there are a number of studies which  
388 have reported the conversion of cellulose I into cellulose II,III or IV after ball milling under specific  
389 conditions [17, 53, 51]. In particular wet ball-milling using water [17, 54, 55, 56] (or NaOH/urea) [53],  
390 even at ambient temperatures (25 °C), can partially transform cellulose I to cellulose II relatively  
391 quickly (e.g. 30 minutes of ball milling). Higher temperatures (e.g. 80 °C and above) can further assist  
392 the transformation, particularly into cellulose IV [17]. The temperature of the powder measured at the  
393 end of the milling step in attrition beads mill was of 70 °C and could explained the change observed in  
394 the crystallinity of the cellulose. In our studies, we haven't measured how temperature evolves during  
395 knife milling.

396 Comminution, by amorphization of particles, results in a decrease in degree of polymerization and  
397 therefore of sample crystallinity. But the comminution process parameters (temperature, humidity,  
398 milling media) also impact cellulose type conversion that are revealed here. These crystallinity  
399 modifications have an effect not only on material sensitivity to moisture absorption but also on sample  
400 thermal stability and adhesion with the polymer matrix and thus composite mechanical properties.

401

## 402 *3.2 Properties of composites*

### 403 *3.2.1 Reinforcement material morphology analysis after processing*

404 Before evaluating the mechanical properties of the **PP-MAPP injection moulded composites processed**  
405 **with 30%-wt reinforcing materials**, the morphology of the reinforcing particles after processing are  
406 given in Figure 6a and b. Figure 6a shows that FF, the 50/50 mix of FF and FS-500 and FS-500 have  
407 important length spans with a median length of 289  $\mu\text{m}$ , 317  $\mu\text{m}$  and 297  $\mu\text{m}$  respectively. The 90<sup>th</sup>  
408 percentile of these samples increases in the same order, indicating an important number of long  
409 particles present in the FS-500 sample which explains that FS-500 + FF has a higher median than  
410 FF itself.

411 The length of FF presents a drastic drop of 70% after processing from their initial length given in figure  
412 1b. The twin-screw extrusion is assumed to be the cause of this as it generates high shear stresses  
413 [20]. Some authors have studied this effect and reported a length reduction between 50% and 70% of  
414 average flax fibre initial length after mono-screw extrusion processing [22, 40]. As shown in Figure 7,  
415 the twin-screws used in this study are designed with several kneading areas, one of them being even  
416 reversed, leading to improved mixing and additional shear stresses. Furthermore, defects in flax fibres,  
417 known as “kink-bands”, have been shown to influence the rupture of fibres during compounding as  
418 localized stress concentrations cause fibre rupture after processing to coincide with the mean distance  
419 between two consecutive kink-bands [57, 58].

420 Surprisingly, FS-500 only underwent a 39% median length reduction due to processing, and an  
421 important quantity of longer particles is present after processing when compared to FF. Shives consist  
422 of fragmented assemblies of xylem cells, which are highly lignified in contrast to fibres. Even so, FS-  
423 250 and WF underwent a 75% and 70% decrease in length respectively, therefore the fragmentation  
424 mechanisms of the FS-500 sample are complicated to judge without further analysis. Moreover, the  
425 proportion of smaller particles is less affected by shear stresses: this is clearly visible in the case of  
426 FS-50 as their length distribution stays practically unchanged with a median length of 20  $\mu\text{m}$  before  
427 and after processing. This suggests that the process may reduce particle length up to a critical length  
428 independent of initial fibre length number of processing cycles.

429 Figure 6b shows the evolution of the distribution of particle aspect ratio before and after processing. It  
430 is possible to see a 36%, 40 % and 77% decrease between Raw-FS and FS-500, FS-250 and FS-50  
431 respectively depending on comminution mode. The median aspect ratio of WF is of 5.5, which is  
432 comparable to that of FS-250, but to the limit that WF shows a higher amount of high aspect ratio  
433 particles, as the WF last decile is of 15.4 against 11.9 for FS-250. After processing of the 30%-wt  
434 reinforced PP-MAPP composites, reinforcement material aspect ratio globally decreases. Indeed, the  
435 L/D of FF and WF decreases by 8% and 11% when compared to before processing, and this is even  
436 more accentuated for FS-500 and FS-250, which show a 21% and 38% drop respectively.  
437 Interestingly, L/D distribution tends to tighten for FS towards smaller values due to the reduction of  
438 particle length because during processing, as discussed earlier.

439 The median aspect ratio of FF is the highest at 11.5 due to the combined action of the delamination  
440 of bundles into individual fibres [37]. For the other reinforcing materials, the median aspect ratios are

441 of 4.8, 3.5 and 2.3 for FS-500, FS-250 and FS-50 respectively, while that of WF is equivalent to FS-  
442 500 at 4.9, although a higher proportion of elongated particle is present as the 84<sup>th</sup> percentile is of 8.4  
443 for WF against 7.3 for FS-500. Flax fibres therefore have a load transfer potential more than twice as  
444 great as wood flour but other parameter must be taken into account such as fibre-matrix adhesion and  
445 the proportion of fines possibly accountable for fracture initiation. The relevance of the 50/50 mixture  
446 of FF and FS-500 is to increase by 30% the median aspect ratio of FS-500 and by up to 110% the last  
447 decile, meaning the potential load transfer of the material is highly improved all the while the price of  
448 the raw material is considerably diminished compared to the initial cut fibres. Indeed, the market value  
449 of raw flax shives can be as low as one thirtieth that of scutched flax fibres. Furthermore, varying  
450 proportions of FS and FF would allow for specific composite mechanical properties all the while  
451 controlling the reinforcing material's cost.

452

### 453 3.2.2 Tensile properties

454 Table 2 shows the tensile mechanical properties of the injected composites of PP-MAPP matrix  
455 reinforced with 30%-wt of the different reinforcing samples. As expected, the incorporation of flax  
456 shives results in a general increase of tensile Young's modulus and maximum strength. The Young's  
457 modulus increases from + 46% to + 112% when FS-50 and FS-500 respectively are compared to the  
458 reference PP-MAPP matrix. FS-500 have a modulus of 3268 ( $\pm$  240) MPa, which is 90 % that of the  
459 FF reinforced composite, and more than a 110% increase in composite rigidity when compared to the  
460 WF reinforced PP-MAPP. Moreover, the addition of flax fibres in the FS-500 reinforcing batch does not  
461 considerably modify the composite's rigidity.

462 Furthermore, the composites have an overall dissimilar ultimate strain. FS-250 and FS-500 have a  
463 comparable behaviour with small ultimate strains of approximately 2.3% as shown Figure 8a and  
464 Table 2. FS-50 and FF+FS-500 both have an ultimate strain 52% higher, while WF and FF exhibit an  
465 increase of 109% and 139% respectively given the ultimate strain of the pure matrix of about 11%.  
466 Finally, FS-50 enables a 27% increase in maximum tensile strength when compared to the initial PP-  
467 MAPP matrix, while FS-250 and FS-500 have a similar behaviour with values around 25 MPa. When a  
468 50/50 mix of FF and FS-500 is incorporated, a 10% increase in tensile strength is noted, reaching and  
469 slightly exceeding that of WF. FS-500 enables the composite to reach almost 80% of the maximum  
470 tensile strength of the reference FF reinforced composite. Figure 8b shows that the maximum tensile

471 strength evolves linearly with particle aspect ratio in the composite, highlighting the close relationship  
472 between particle morphology and composite tensile strength. Therefore, flax shives have an effective  
473 reinforcing potential in PP-MAPP composites and cannot be considered as simply 'fillers' since both  
474 the modulus and maximum tensile strength are enhanced compared to the sole matrix.

475 A comparative graph is shown Figure 9, presenting the mechanical properties of injected  
476 polypropylene composites manufactured with a similar process involving an equivalent twin-screw  
477 extruder. As mentioned previously, the use of fines obtained either from flax fibres or flax shives (FS-  
478 50) increases composite stiffness in a similar manner with a slight advantage for FS-50 which  
479 increases composite strength at break by 14%. Wood flour and FS-250 have analogue Young's  
480 modulus between 2.8 GPa and 2.9 GPa respectively. Our values of flax fibre reinforced injected  
481 composites are in agreement with previous work from the literature.

482

### 483 3.2.3 Role of volume fraction on composite properties

484 Since FS-500 provides the most efficient mechanical properties among the different shive reinforced  
485 batches, it was chosen to investigate the influence of volume fractions on composite mechanical  
486 properties. Figure 10 represents the evolution of both the maximum tensile strength and the  
487 composite's Young modulus as a function of the volume fraction of FS-500. Young's modulus  
488 increases linearly with increasing volume fraction (linear fit with  $R^2 = 0.94$ ), highlighting their  
489 reinforcing potential. Furthermore, the maximum tensile strength increases with increasing volume  
490 fraction up to about 23%-vol of FS-500 and then decreases above this volume fraction. This behaviour  
491 is similar to that of other plant cell wall reinforcing materials, such as flax fibres for which the optimum  
492 tensile strength in PP-MAPP injection moulded composites is situated at an optimum volume fraction  
493 around 33% [20]. **We hypothesises that above this volume fraction, particles become too short to  
494 effectively reinforce de polymer matrix, presumably due to increasing shear rates induced by particle-  
495 particle friction during processing [61].**

496 The fibre aspect ratio decreases during processing with increasing fibre volume fraction due to  
497 increasing induced shear rates [59]. In our case, FS-500 aspect ratio after processing is only 4.8 for  
498 the 23%-vol fraction against approximately 20 for the flax fibres used in the study of Ausias et al. [20]  
499 for a comparable 20% fibre volume fraction; keeping in mind that in their study the initial fibre length

500 was of 2 mm and that only one step of single-screw extrusion was carried out prior to injection  
 501 moulding; and this manufacturing process causes fibres to be randomly dispersed in the samples.

502

### 503 3.2.4 Analysis of the critical aspect ratio

504 When considering a unidirectional composite reinforced by short fibres assumed to be parallel to the  
 505 applied stress, fibre aspect ratio will influence its tensile strength at break [62]. Assuming that i) the  
 506 applied load must be transferred to the fibre by the fibre-matrix interface, ii) no loads are transferred at  
 507 the fibre's section, iii) shear stresses are constant along the fibre's length, iv) the matrix's strain at  
 508 break is considerably higher than that of the fibres, v) both the matrix and the reinforcing fibres have  
 509 an elastic and linear behaviour, and vi) the fibres are solid cylinders, Kelly and Tyson established a  
 510 simplified model [63] defining the critical fibre length  $L_c$  as follows (Eq. 3) :

$$511 \quad L_c = \frac{\sigma_{f,u} d}{2 \tau_i} \quad \text{Eq. 3}$$

512 Where  $\sigma_{f,u}$  is the ultimate fibre stress,  $d$  the fibre diameter and  $\tau_i$  is shear stress at the fibre-matrix  
 513 interface. The calculation details can be found in different composite literature, by Gibson for instance  
 514 [62]. The critical aspect ratio can then be considered as the minimal aspect ratio for a fibre to break  
 515 without pull-out.

516 SEM images of the fracture surface of PP-MAPP and FS-500 composites (Figure 11) shows that some  
 517 large particles maintain their alveolar cell structure even after processing, and that the matrix is able to  
 518 penetrate in it. Furthermore, it even appears that in some places rupture takes place through the flax  
 519 shive particles due to matrix infiltration (Fig. 11b).

520 Let us consider FS as a tubular structure in which the elementary volumes, immersed in matrix, have a  
 521 central lumen completely impregnated by the polymer, as shown in Figure 11b. FS can be simplified  
 522 as a hollow cylinder having a length  $L$ , an average diameter  $\bar{d}_f$  and a thickness  $e$ . In a similar  
 523 reasoning as previous, tubes are considered to be parallel to one another in a unidirectional  
 524 composite. Let's consider  $d_x$ , an infinitely small portion of this hollow cylinder along the  $x$  axis being  
 525 fully impregnated with the polymer matrix (as shown in Figure 12), and that the cylinder is parallel to a  
 526 tensile solicitation of the composite. If we consider, as did Kelly and Tyson, that reinforcing is done in  
 527 the form of shear stresses considered to be constant along cylinder's length, then the forces applied to  
 528 the cylinder can be summarized as follows (Eq. 4):

$$529 \quad (\sigma_{cw} + d\sigma_{cw})S = \sigma_{cw}S + \tau_{i,ins}(\bar{d}_f + e)d_x + \tau_{i,ext}(\bar{d}_f - e)d_x \quad \text{Eq. 4}$$

530 With  $\sigma_{cw}$  the tensile strength applied to the cylinder's surface  $S$ ,  $\tau_e$  the shear stresses applied on its  
531 external surface and  $\tau_i$  those applied to its inside.

532 Since the matrix is considered to have an elastic behaviour, then  $\tau_{i,ins} = \tau_{i,ext}$ , and when resolving  
533 this equation based on the Kelly-Tyson model by integration along the cylinder's length, then the  
534 previous equation (Eq.4) becomes equation 5, and the critical length at which tensile strength causes  
535 cell wall rupture does not depend on fibre diameter (as previously established in equation 3), but  
536 rather on the cell wall thickness.

$$537 \quad L_c = \frac{\sigma_{cw,u} * e}{\tau_i} \quad \text{Eq. 5}$$

538 To the best of our knowledge, the average flax xylem cell wall tensile strength has not been reported  
539 in the literature. If we consider that flax shives are mainly made of secondary xylem with a composition  
540 and structure similar to that of wood, then we can assume that the tensile yield strength of the cell  
541 walls of flax shives is also similar to that of gymnosperm earlywood which was measured to be  
542 350 MPa for *Pinus Radiata* [64]. In ongoing studies, we measured the global cell wall thickness in flax  
543 xylem to be of 2.4  $\mu\text{m}$  on average by SEM observations of a stem's transverse section. Merotte et al.  
544 [65] measured an interfacial shear strength (IFSS) between flax and MAPP of  $10.6 \pm 2.8$  MPa.  
545 Therefore, the critical length of a tubular structure assimilated to FS is estimated to be about 79  $\mu\text{m}$   
546 (Eq. 5); against 526  $\mu\text{m}$  estimated using the Kelly-Tyson model (Eq. 3) for a solid-section flax fibre of  
547 15  $\mu\text{m}$  in diameter and an ultimate strength at break of 950 MPa [66]. This is a 6.7 times lower critical  
548 length when using this simplistic model, showing the potential reinforcing efficiency of particles which  
549 may be considered as fines (less than 200  $\mu\text{m}$  in length) but having a hollow structure, due to the  
550 importance of cell wall thickness rather than aspect ratio.

551 Clearly, in this simplified model the lumen is considered to fully impregnated, and cell wall orientation,  
552 matrix wetting and cell wall-matrix adhesion are just a few parameters that might influence shear  
553 stresses inside and outside of the tubular cell wall, which may therefore not be equal in reality.

554 Furthermore, cell wall thickness in the xylem evolves with cell wall type, plant maturity and along a flax  
555 stem, whereas FS are an assembly of all these different elements creating a gradient in reinforcing  
556 potential. Additionally, the assumption that cells are circular is preferred for estimation purposes, but  
557 cell wall most often have a polygonal transversal shape that should also be accounted for. This makes  
558 FS fragmentation a determining factor for hollow cell accessibility by the matrix.

559

560

#### 561 **4. Conclusion**

562 This study focused on the reinforcement potential of flax shives in PP-MAPP injection moulded  
563 composites following the investigation of the fragmented by-product materials. The granulometry  
564 analysis succeeding raw FS comminution highlights the importance of the mode of particle size  
565 analysis which can easily hide small particles or fines. The volume distribution of fragmented flax  
566 shives shows that the FS-250 and FS-500 batches are comprised of a high number of particles having  
567 a well conserved alveolar structure. Due to the nature of cells, FS have a different biochemical  
568 composition than flax fibres as the former contain less than half the latter's amount of cellulose and  
569 around six times the latter's amount of lignin. The composition of FS does not evolve with  
570 fragmentation, even after an intense attrition-beads milling process. However, the crystallinity index of  
571 FS decreases with comminution up to a 50% for the severely transformed FS-50 due to amorphization  
572 of particles resulting in a decrease in degree of polymerization and therefore sample crystallinity, as  
573 well as a conversion of crystalline cellulose I into cellulose II or III.

574 Following this preliminary study, the tensile mechanical properties of injection moulded PP-MAPP  
575 composites were evaluated. Compounding and injection moulding induced a 70% decrease in flax  
576 fibre and FS-250 length but did not modify the length of FS-50 due to their initially small particle size.  
577 The tensile maximum strength of the composites increases linearly with particle aspect ratio, and  
578 interestingly, FS-500 tensile Young's modulus reaches 90% that of the reference FF composite. The  
579 FS-500 sample presented the best mechanical properties among the other fragmented FS batches  
580 and was chosen to further analyse the consequences of FS volume fraction. Unlike flax fibres, FS-500  
581 present an optimal tensile strength at 23% in volume fraction, against 33%-vol for flax fibres. SEM  
582 observations reveal that the matrix is able to penetrate in some flax shives having a tubular structure.  
583 In the case of a hollow cylinder fully impregnated by the matrix, we have shown that the critical length  
584 of the particle depends not on particle diameter but rather on tube wall thickness, highlighting the  
585 reinforcing potential of hollow fines. The study shows the legitimacy of flax shives as reinforcing  
586 material in the field of biocomposites.

587

588        **5. Acknowledgments**

589        The authors would like to thank the National Association of Research and Technology for financing a  
590        thesis in partnership with Van Robaeys Frères and the Dupuy de Lôme Research Institute of the  
591        South Brittany University (France). Furthermore, authors would like to thank Gwendoline Guillouroux  
592        and Maelenn le Gall from IFREMER for their valuable work, as well as Sylviane Daniel from INRA for  
593        her kindness with biochemical analysis and Philippe Violle from Sympatec for his availability and good  
594        guidance on the project.

595

596 References:

- 597 [1] J. Beaugrand, M. Nottez, J. Konnerth, and A. Bourmaud, "Multi-scale analysis of the structure  
598 and mechanical performance of woody hemp core and the dependence on the sampling  
599 location," *Ind. Crops Prod.*, vol. 60, pp. 193–204, 2014.
- 600 [2] T. Väisänen, A. Haapala, R. Lappalainen, and L. Tomppo, "Utilization of agricultural and forest  
601 industry waste and residues in natural fiber-polymer composites : A review," *Waste Manag.*,  
602 vol. 54, pp. 62–73, 2016.
- 603 [3] A. O. Ogah and J. N. Afiukwa, "Characterization and comparison of mechanical behavior of  
604 agro fiber-filled high-density polyethylene bio-composites," *J. Reinf. Plast. Compos.*, vol. 33,  
605 pp. 37–46, 2014.
- 606 [4] A. Le Duigou, J. M. Deux, P. Davies, and C. Baley, "PLLA/flax mat/balsa bio-sandwich-  
607 environmental impact and simplified life cycle analysis," *Appl. Compos. Mater.*, vol. 19, no. 3–4,  
608 pp. 363–378, 2012.
- 609 [5] M. Pervaiz and M. M. Sain, "Carbon storage potential in natural fiber composites," *Resour.*  
610 *Conserv. Recycl.*, vol. 39, no. 4, pp. 325–340, 2003.
- 611 [6] S. Réquillé, C. Goudenhoft, A. Bourmaud, A. Le Duigou, and C. Baley, "Exploring the link  
612 between flexural behaviour of hemp and flax stems and fibre stiffness," *Ind. Crops Prod.*, vol.  
613 113, no. January, pp. 179–186, 2018.
- 614 [7] F. Bert, "Lin fibre: Culture et transformation," *Arvalis-Institut du Végétal Paris, Fr.*, 2013.
- 615 [8] J. Foulk, D. E. Akin, R. Dodd, and C. Ulven, "Production of Flax Fibers for Biocomposites," in  
616 *Cellulose Fibers: Bio- and Nano-Polymer Composites*, Berlin, Heidelberg: Springer Berlin  
617 Heidelberg, 2011, pp. 61–95.
- 618 [9] W. E. Marshall, L. H. Wartelle, and D. E. Akin, "Flax shive as a source of activated carbon for  
619 metals remediation," *BioResources*, vol. 2, pp. 82–90, 2007.
- 620 [10] V. Dubois, A. Leblanc, O. Carpentier, G. Alhaik, and E. Wirquin, "Performances of flax shive-  
621 based lightweight composites with rapid hardening," *Constr. Build. Mater.*, vol. 165, pp. 17–27,  
622 2018.
- 623 [11] S. González-García, L. Luo, M. T. Moreira, G. Feijoo, and G. Huppés, "Life cycle assessment  
624 of flax shives derived second generation ethanol fueled automobiles in Spain," *Renew. Sustain.*  
625 *Energy Rev.*, vol. 13, no. 8, pp. 1922–1933, Oct. 2009.

- 626 [12] C. Goudenhooff, A. Bourmaud, and C. Baley, "Varietal selection of flax over time: Evolution of  
627 plant architecture related to influence on the mechanical properties of fibers," *Ind. Crops Prod.*,  
628 vol. 97, pp. 56–64, 2017.
- 629 [13] W. Hu, M. Zhang, M. T. Ton-That, and T. dung Ngo, "A comparison of flax shive and extracted  
630 flax shive reinforced PP composites," *Fibers Polym.*, vol. 15, no. 8, pp. 1722–1728, 2014.
- 631 [14] A. Day *et al.*, "Lignification in the flax stem: Evidence for an unusual lignin in bast fibers,"  
632 *Planta*, vol. 222, no. 2, pp. 234–245, 2005.
- 633 [15] N. Chevanan, A. R. Womac, V. S. Bitra, and S. Sokhansanj, "Effect of Particle Size Distribution  
634 on Loose-filled and Tapped Densities of Selected Biomass after Knife Mill Size Reduction,"  
635 *Appl. Eng. Agric.*, vol. 27, no. 4, pp. 631–644, 2011.
- 636 [16] C. Mayer-Laigle, R. Rajaonarivony, N. Blanc, and X. Rouau, "Comminution of Dry  
637 Lignocellulosic Biomass: Part II. Technologies, Improvement of Milling Performances, and  
638 Security Issues," *Bioengineering*, vol. 5, no. 3, p. 50, 2018.
- 639 [17] J. A. Howsmon and R. H. Marchessault, "The ball-milling of cellulose fibers and  
640 recrystallization effects," *J. Appl. Polym. Sci.*, vol. 1, no. 3, pp. 313–322, May 1959.
- 641 [18] T. Qiang, J. Wang, and M. P. Wolcott, "Facile Preparation of Cellulose/Poly lactide Composite  
642 Materials with Tunable Mechanical Properties," *Polym. - Plast. Technol. Eng.*, vol. 57, no. 13,  
643 pp. 1288–1295, 2018.
- 644 [19] A. K. Bledzki, A. A. Mamun, and O. Faruk, "Abaca fibre reinforced PP composites and  
645 comparison with jute and flax fibre PP composites," *Express Polym. Lett.*, vol. 1, no. 11, pp.  
646 755–762, 2007.
- 647 [20] G. Ausias, A. Bourmaud, G. Coroller, and C. Baley, "Study of the fibre morphology stability in  
648 polypropylene-flax composites," *Polym. Degrad. Stab.*, vol. 98, no. 6, pp. 1216–1224, 2013.
- 649 [21] A. Bourmaud, A. Le Duigou, and C. Baley, "Mechanical performance of flax-based  
650 biocomposites," in *Biocomposites*, Fourteenth., Elsevier Ltd., 2015, pp. 365–399.
- 651 [22] M. Tanguy, A. Bourmaud, J. Beaugrand, T. Gaudry, and C. Baley, "Polypropylene  
652 reinforcement with flax or jute fibre; Influence of microstructure and constituents properties on  
653 the performance of composite," *Compos. Part B Eng.*, vol. 139, no. November 2016, pp. 64–  
654 74, 2018.
- 655 [23] N. Graupner, G. Ziegmann, F. Wilde, F. Beckmann, and J. Müssig, "Procedural influences on

- 656 compression and injection moulded cellulose fibre-reinforced polylactide (PLA) composites:  
657 Influence of fibre loading, fibre length, fibre orientation and voids," *Compos. Part A Appl. Sci.*  
658 *Manuf.*, vol. 81, pp. 158–171, 2016.
- 659 [24] A. Bourmaud, G. Ausias, G. Lebrun, M. Tachon, and C. Baley, "Observation of the structure of  
660 a composite polypropylene / flax and damage mechanisms under stress," *Ind. Crop. Prod.*, vol.  
661 43, pp. 225–236, 2013.
- 662 [25] N. M. Stark and R. E. Rowlands, "Effects of wood fiber characteristics on mechanical  
663 properties of wood/polypropylene composites," *Wood fiber Sci. Vol. 35, no. 2 Pages 167-174*,  
664 2003.
- 665 [26] K. Albrecht, T. Osswald, E. Baur, T. Meier, S. Wartzack, and J. Müssig, "Fibre Length  
666 Reduction in Natural Fibre-Reinforced Polymers during Compounding and Injection Moulding—  
667 Experiments Versus Numerical Prediction of Fibre Breakage," *J. Compos. Sci.*, vol. 2, no. 2, p.  
668 20, Mar. 2018.
- 669 [27] N. Martin, N. Mouret, P. Davies, and C. Baley, "Influence of the degree of retting of flax fibers  
670 on the tensile properties of single fibers and short fiber/polypropylene composites," *Ind. Crops*  
671 *Prod.*, vol. 49, pp. 755–767, 2013.
- 672 [28] M. H. B. Snijder and H. L. Bos, "Reinforcement of polypropylene by annual plant fibers:  
673 Optimisation of the coupling agent efficiency," *Compos. Interfaces*, vol. 7, no. 2, pp. 69–75,  
674 2000.
- 675 [29] G. Coroller, "Contribution à l'étude des matériaux composites renforcés par des fibres  
676 végétales: cas des composites extrudés à matrice polypropylène," Lorient, 2013.
- 677 [30] C. Mayer-Laigle, N. Blanc, R. Rajaonarivony, and X. Rouau, "Comminution of Dry  
678 Lignocellulosic Biomass, a Review: Part I. From Fundamental Mechanisms to Milling  
679 Behaviour," *Bioengineering*, vol. 5, no. 2, p. 41, 2018.
- 680 [31] J. F. Thibault, "Automatisation du dosage des substances pectiques par la methode au meta-  
681 hydroxydiphenyl," *Lebensmittel - Wissenschaft + Technologie. Food science + technology*, vol.  
682 v. 12. 1979.
- 683 [32] A. B. Blakeney, P. J. Harris, R. J. Henry, and B. A. Stone, "A simple and rapid preparation of  
684 alditol acetates for monosaccharide analysis," *Carbohydr. Res.*, vol. 113, no. 2, pp. 291–299,  
685 Mar. 1983.

- 686 [33] R. Hatfield and R. S. Fukushima, "Can lignin be accurately measured?," *Crop Sci.*, vol. 45, no.  
687 3, pp. 832–839, 2005.
- 688 [34] L. Segal, J. J. Creely, A. E. Martin, and C. M. Conrad, "An Empirical Method for Estimating the  
689 Degree of Crystallinity of Native Cellulose Using the X-Ray Diffractometer," *Text. Res. J.*, vol.  
690 29, no. 10, pp. 786–794, Oct. 1959.
- 691 [35] S. Park, J. O. Baker, M. E. Himmel, P. A. Parilla, and D. K. Johnson, "Cellulose crystallinity  
692 index: measurement techniques and their impact on interpreting cellulase performance,"  
693 *Biotechnol. Biofuels*, vol. 3, no. 1, p. 10, 2010.
- 694 [36] M. Le Gall, P. Davies, N. Martin, and C. Baley, "Recommended flax fibre density values for  
695 composite property predictions," *Ind. Crops Prod.*, vol. 114, no. February, pp. 52–58, 2018.
- 696 [37] N. Le Moigne, M. Van Den Oever, and T. Budtova, "A statistical analysis of fibre size and  
697 shape distribution after compounding in composites reinforced by natural fibres," *Compos. Part*  
698 *A*, vol. 42, no. 10, pp. 1542–1550, 2011.
- 699 [38] L. Teuber, H. Militz, and A. Krause, "Dynamic particle analysis for the evaluation of particle  
700 degradation during compounding of wood plastic composites," *Compos. Part A Appl. Sci.*  
701 *Manuf.*, vol. 84, pp. 464–471, 2016.
- 702 [39] K. Haag and J. Müssig, "Scatter in tensile properties of flax fibre bundles : influence of  
703 determination and calculation of the cross- sectional area," *J. Mater. Sci.*, vol. 51, pp. 7907–  
704 7917, 2016.
- 705 [40] E. Di Giuseppe *et al.*, "Reliability evaluation of automated analysis, 2D scanner, and micro-  
706 tomography methods for measuring fiber dimensions in polymer-lignocellulosic fiber  
707 composites," *Compos. Part A Appl. Sci. Manuf.*, vol. 90, pp. 320–329, Nov. 2016.
- 708 [41] A. Bourmaud, C. Mayer-Laigle, C. Baley, and J. Beaugrand, "About the frontier between filling  
709 and reinforcement by fine flax particles in plant fibre composites," *Ind. Crops Prod.*, vol. 141,  
710 no. September, p. 111774, Dec. 2019.
- 711 [42] P. Evon *et al.*, "Production of fiberboards from shives collected after continuous fiber  
712 mechanical extraction from oleaginous flax," *J. Nat. Fibers*, vol. 00, no. 00, pp. 1–17, Jan.  
713 2018.
- 714 [43] C. Goudenhooff, "Multi-scale characterization of flax stems and fibers : structure and  
715 mechanical performances," 2018.

- 716 [44] P. Trivelato, C. Mayer, A. Barakat, H. Fulcrand, and C. Aouf, "Douglas bark dry fractionation for  
717 polyphenols isolation : From forestry waste to added value products," *Ind. Crop. Prod.*, vol. 86,  
718 pp. 12–15, 2016.
- 719 [45] A. U. Buranov, K. A. Ross, and G. Mazza, "Isolation and characterization of lignins extracted  
720 from flax shives using pressurized aqueous ethanol," *Bioresour. Technol.*, vol. 101, no. 19, pp.  
721 7446–7455, 2010.
- 722 [46] T. A. Gorshkova *et al.*, "Specific type of secondary cell wall formed by plant fibers," *Russ. J.*  
723 *Plant Physiol.*, vol. 57, no. 3, pp. 328–341, 2010.
- 724 [47] G. Değer, M. Pakdemirli, F. Candan, S. Akgün, and H. Boyacı, "Strength of Wheat and Barley  
725 Stems and Design of New Beam/Columns," *Math. Comput. Appl.*, vol. 15, no. 1, pp. 1–13, Apr.  
726 2010.
- 727 [48] R. C. Pettersen, "The chemical composition of wood," in *The chemistry of solid wood*, CRC  
728 Press, 1985, pp. 57–126.
- 729 [49] A. D. French, "Idealized powder diffraction patterns for cellulose polymorphs," *Cellulose*, vol.  
730 21, no. 2, pp. 885–896, 2014.
- 731 [50] A. S. Khan *et al.*, "Impact of Ball-Milling Pretreatment on Pyrolysis Behavior and Kinetics of  
732 Crystalline Cellulose," *Waste and Biomass Valorization*, vol. 7, no. 3, pp. 571–581, 2015.
- 733 [51] C. M. Lee *et al.*, "Cellulose polymorphism study with sum-frequency-generation (SFG) vibration  
734 spectroscopy: identification of exocyclic CH<sub>2</sub>OH conformation and chain orientation," *Cellulose*,  
735 vol. 20, no. 3, pp. 991–1000, Jun. 2013.
- 736 [52] Z. Tang *et al.*, "TEMPO-Oxidized cellulose with high degree of oxidation," *Polymers (Basel)*,  
737 vol. 9, no. 9, pp. 3–4, 2017.
- 738 [53] C. C. Piras, S. Fernández-Prieto, and W. M. De Borggraeve, "Ball milling: a green technology  
739 for the preparation and functionalisation of nanocellulose derivatives," *Nanoscale Adv.*, pp.  
740 937–947, 2019.
- 741 [54] L. Y. Yatsu, T. A. Calamari, and R. R. Benerito, "Conversion of Cellulose I to Stable Cellulose  
742 III," *Text. Res. J.*, vol. 56, no. 7, pp. 419–424, 1986.
- 743 [55] M. Ago, T. Endo, and T. Hirotsu, "Crystalline transformation of native cellulose from cellulose I  
744 to cellulose II polymorph by a ball-milling method with a specific amount of water," *Cellulose*,  
745 vol. 11, no. 2, pp. 163–167, 2004.

- 746 [56] V. Kocherbitov, S. Ulvenlund, M. Kober, K. Jarring, and T. Arnebran, "Hydration of  
747 microcrystalline cellulose and milled cellulose studied by sorption calorimetry," *J. Phys. Chem.*  
748 *B*, vol. 112, no. 12, pp. 3728–3734, 2008.
- 749 [57] S. T. Su, J. Xiong, and J. Ye, "Effect of Ball Milling on Structure of Microcrystalline Cellulose,"  
750 *Appl. Mech. Mater.*, vol. 394, pp. 201–204, 2013.
- 751 [58] X. H. Liang, L. Z. Gu, and E. Y. Ding, "Recrystallization behavior of cellulose and lignocellulose  
752 from *Pinus massoniana*," *Wood Sci. Technol.*, vol. 27, no. 6, pp. 461–467, 1993.
- 753 [59] A. Le Duc, B. Vergnes, and T. Budtova, "Polypropylene/natural fibres composites: Analysis of  
754 fibre dimensions after compounding and observations of fibre rupture by rheo-optics," *Compos.*  
755 *Part A Appl. Sci. Manuf.*, vol. 42, no. 11, pp. 1727–1737, 2011.
- 756 [60] C. Gourier, A. Bourmaud, A. Le Duigou, and C. Baley, "Influence of PA11 and PP  
757 thermoplastic polymers on recycling stability of unidirectional flax fibre reinforced  
758 biocomposites," *Polym. Degrad. Stab.*, vol. 136, pp. 1–9, 2017.
- 759 [61] D. M. Bigg, D. F. Hiscock, J. R. Preston, and E. J. Bradbury, "Thermoplastic matrix sheet  
760 composites," *Polym. Compos.*, vol. 9, no. 3, pp. 222–228, Jun. 1988.
- 761 [62] R. F. Gibson, *Principles of Composite Material Mechanics*. 1994.
- 762 [63] A. Kelly and W. R. Tyson, "Tensile Properties of Fibre-Reinforced Metals: Copper/Tungsten  
763 and Copper/Molybdenum," *J. Mech. Phys. Solids*, vol. 13, pp. 329–350, 1965.
- 764 [64] I. D. Cave, "The longitudinal Young's modulus of *Pinus radiata*," *Wood Sci. Technol.*, vol. 3, no.  
765 1, pp. 40–48, 1969.
- 766 [65] J. Merotte *et al.*, "Flax and hemp nonwoven composites : The contribution of interfacial bonding  
767 to improving tensile properties," *Polym. Test.*, vol. 66, pp. 303–311, 2018.
- 768 [66] C. Baley and A. Bourmaud, "Average tensile properties of French elementary flax fibers,"  
769 *Mater. Lett.*, vol. 122, pp. 159–161, 2014.

770

771

772

773

774

775

776 FIGURE CAPTIONS

777 **Figure 1.** Reinforcing material length distribution after comminution a) in number, b) in volume. The  
778 10<sup>th</sup> (first decile), 16<sup>th</sup>, 50<sup>th</sup> (median), 84<sup>th</sup>, and 90<sup>th</sup> (last decile) percentiles of the cumulative  
779 distribution in length are shown respectively from bottom up with corresponding values of 16<sup>th</sup>, 50<sup>th</sup>  
780 and 84<sup>th</sup> percentiles facing them.

781 **Figure 2.** Length distribution of reinforcing materials and visual aspect as observed with SEM.

782 **Figure 3.** Preserved cell wall alveolar structure of some FS-250 particles after comminution. Arrow  
783 points to an interesting tracheary element of the flax xylem.

784 **Figure 4.** Analysis of lignin, glucose and non-glucosidic monosaccharide content of reinforcing  
785 materials.

786 **Figure 5.** a) XRD spectra for the ball milled flax shives (raw, 50, 250, 500). For reference, the XRD  
787 spectra of Avicel cellulose from Lee et al. [49] marked with \* on the graph are also illustrated. b) The  
788 evolution in the crystallinity of the samples.

789 **Figure 6.** a) Particle length distribution in volume and b) Aspect ratios of extracted materials. The  
790 10<sup>th</sup> (first decile), 16<sup>th</sup>, 50<sup>th</sup> (median), 84<sup>th</sup>, and 90<sup>th</sup> (last decile) percentiles of the cumulative  
791 distribution in length are shown respectively from bottom up with the 16<sup>th</sup>, 50<sup>th</sup> and 84<sup>th</sup> percentile  
792 values facing them.

793 **Figure 7.** Screw design of the twin screws used for extrusion, with both transportation areas (white)  
794 and kneading areas (grey). Screw length L/D is 40, flow direction is from right to left.

795 **Figure 8.** a) Typical tensile stress and deformation behaviour of 30%-wt reinforced PP-MAPP  
796 composites, b) Maximum tensile strength of PP-MAPP reinforced composite as function of reinforcing  
797 material aspect ratio.

798 **Figure 9.** Comparison of mechanical properties provided by different reinforcing materials. For all the  
799 batches of this study, both PP-MAPP matrix and extrusion machine are the same. Samples marked  
800 with \* are obtained from [40].

801 **Figure 10.** The Young's modulus and maximum tensile strength of FS-500 reinforced composite as  
802 function of volume fraction.

803 **Figure 11.** a) Fracture surface of the FS-500 reinforced PP-MAPP composite b) Highlight of a  
804 potential matrix penetration in the alveolar structure. Arrows indicate cell-walls.

805 **Figure 12.** Schematic representation of the mechanical forces applied to a hollow tubular short cell  
806 wall structure in a polymer matrix during tensile testing.

807

808 TABLE CAPTIONS

809 **Table 1.** Reinforcing material samples and corresponding abbreviations.

810 **Table 2.** Tensile properties of injected composites reinforced with 30%-wt reinforcing materials.

811

812

Color should be used for all figures in manuscript.

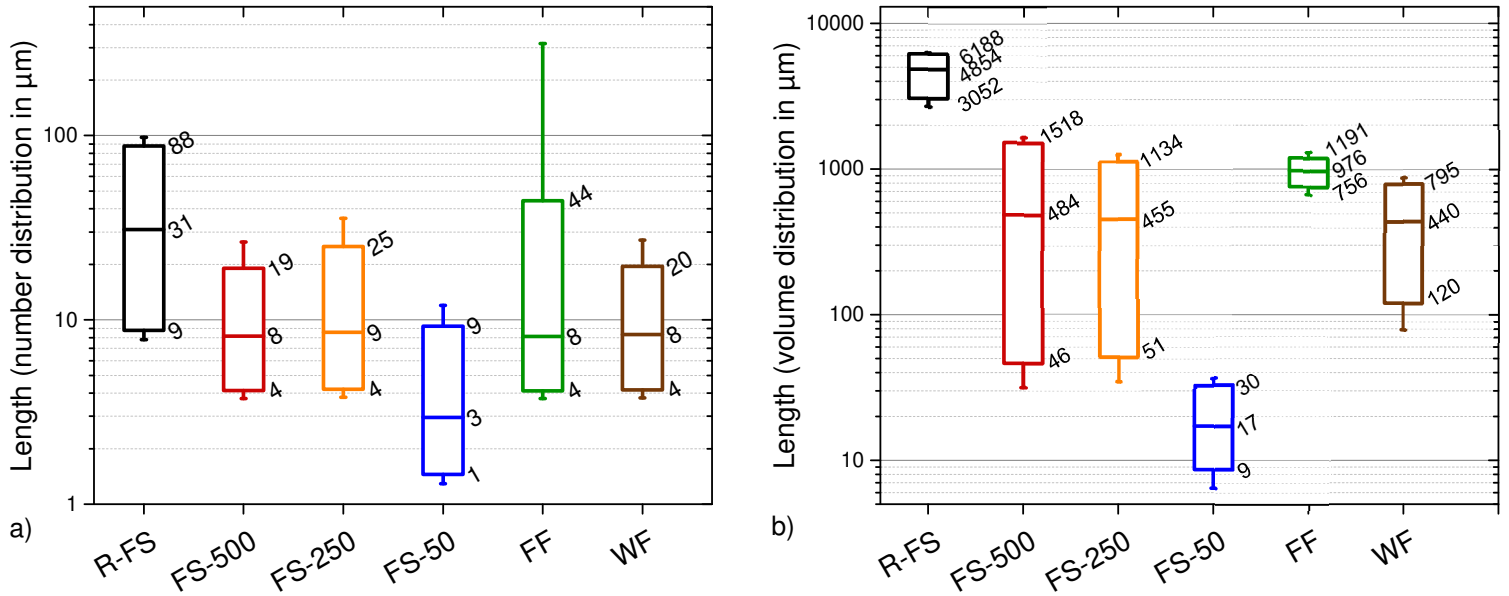


Figure 1. Reinforcing material length distribution after comminution a) in number, b) in volume. The 10<sup>th</sup> (first decile), 16<sup>th</sup>, 50<sup>th</sup> (median), 84<sup>th</sup>, and 90<sup>th</sup> (last decile) percentiles of the cumulative distribution in length are shown respectively from bottom up with corresponding values of 16<sup>th</sup>, 50<sup>th</sup> and 84<sup>th</sup> percentiles facing them.

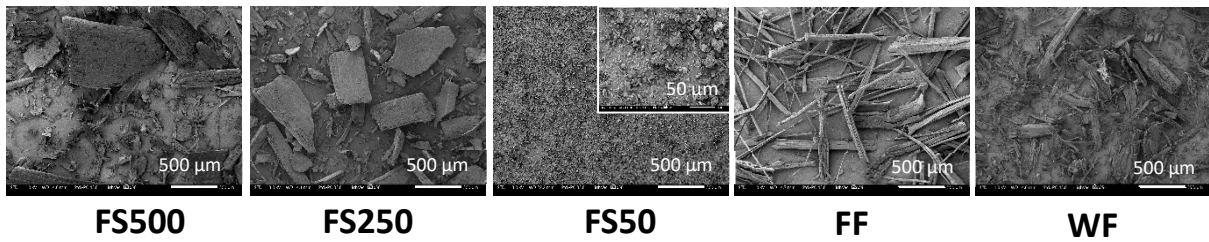
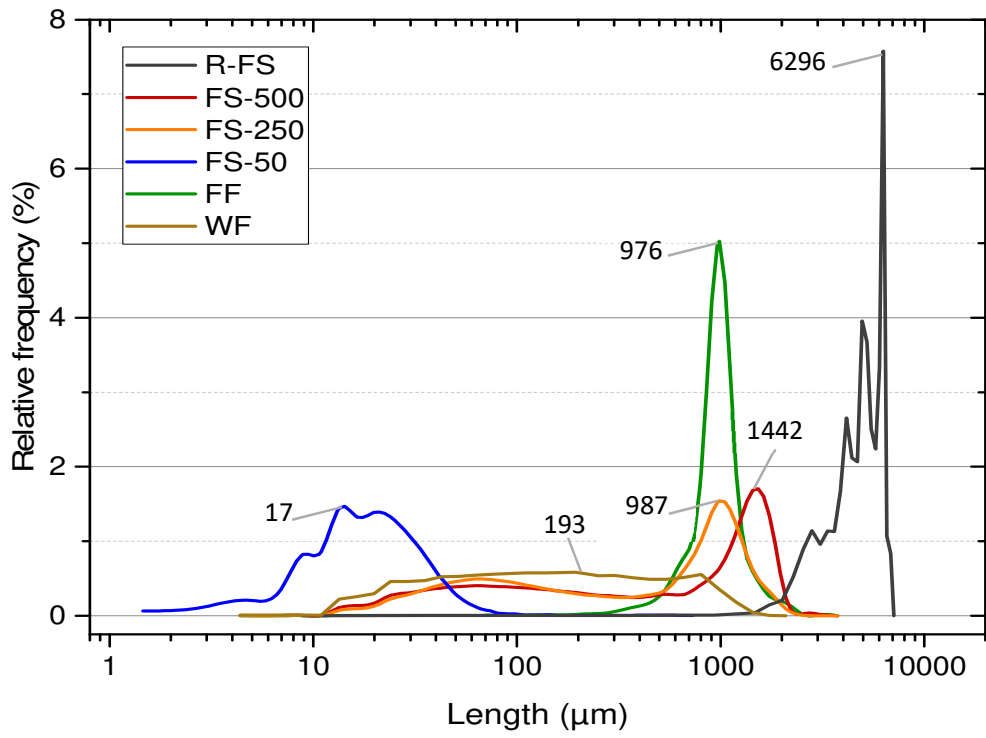
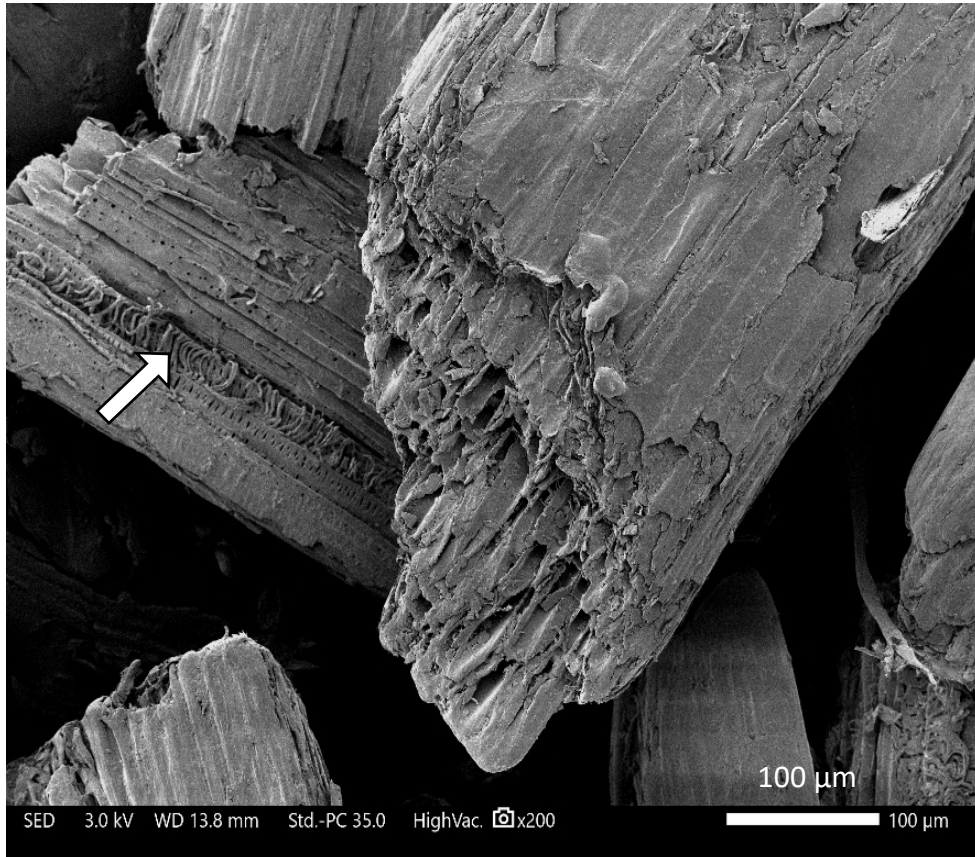


Figure 2. Length distribution of reinforcing materials and visual aspect as observed with SEM.



*Figure 3. Preserved cell wall alveolar structure of some FS-250 particles after comminution. Arrow points to an interesting tracheary element of the flax xylem.*

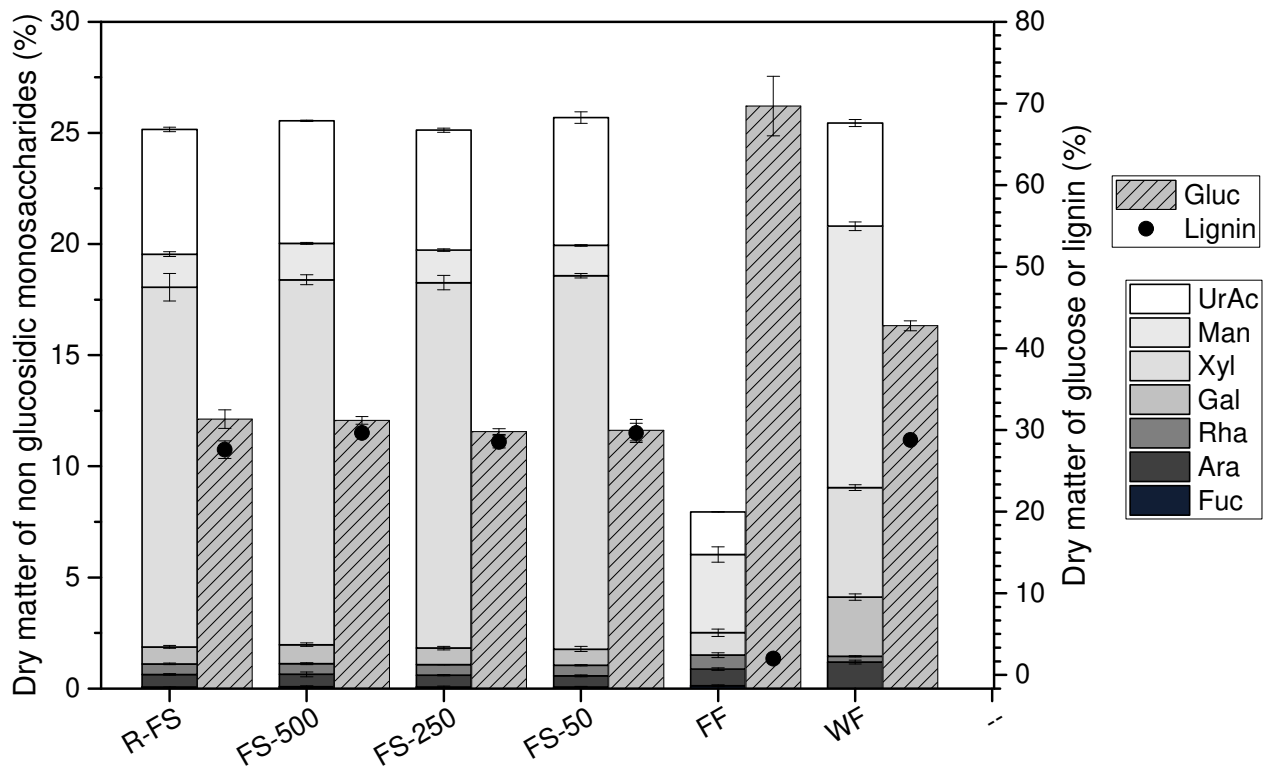


Figure 4. Analysis of lignin, glucose and non-glucosidic monosaccharide content of reinforcing materials.

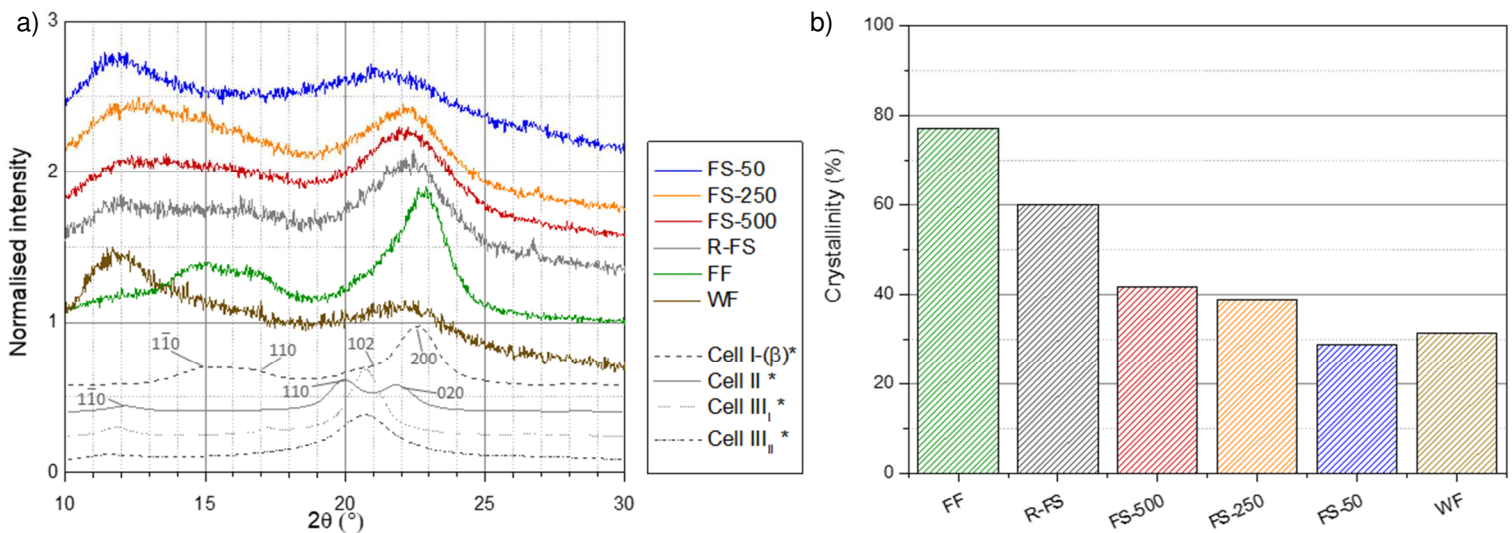


Figure 5. a) XRD spectra for the **fragmented** flax shives (raw, 50, 250, 500). For reference, the XRD spectra of Avicel cellulose from Lee et al. [49] marked with \* on the graph are also illustrated. b) The evolution in the crystallinity of the samples.

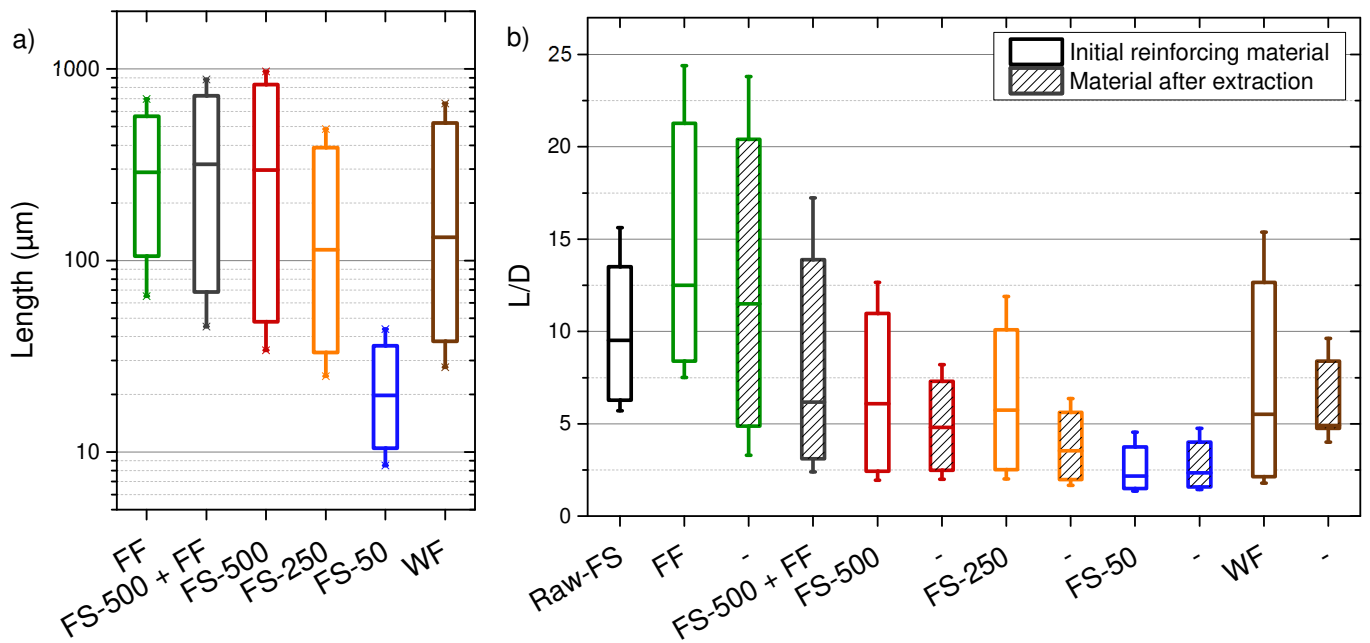


Figure 6. a) Particle length distribution in volume and b) Aspect ratios of *initial reinforcing material compared to extracted materials from the 30%-wt reinforced PP-MAPP composite*. The 10<sup>th</sup> (first decile), 16<sup>th</sup>, 50<sup>th</sup> (median), 84<sup>th</sup>, and 90<sup>th</sup> (last decile) percentiles of the cumulative distribution in length are shown respectively from bottom up.

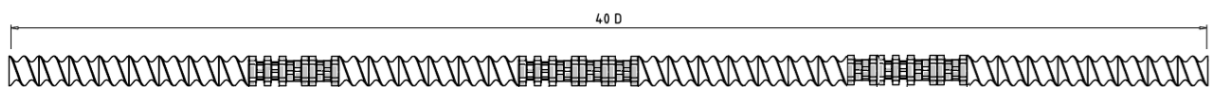


Figure 7. Screw design of the twin screws used for extrusion, with both transportation areas (white) and kneading areas (grey). Screw length  $L/D$  is 40, flow direction is from right to left.

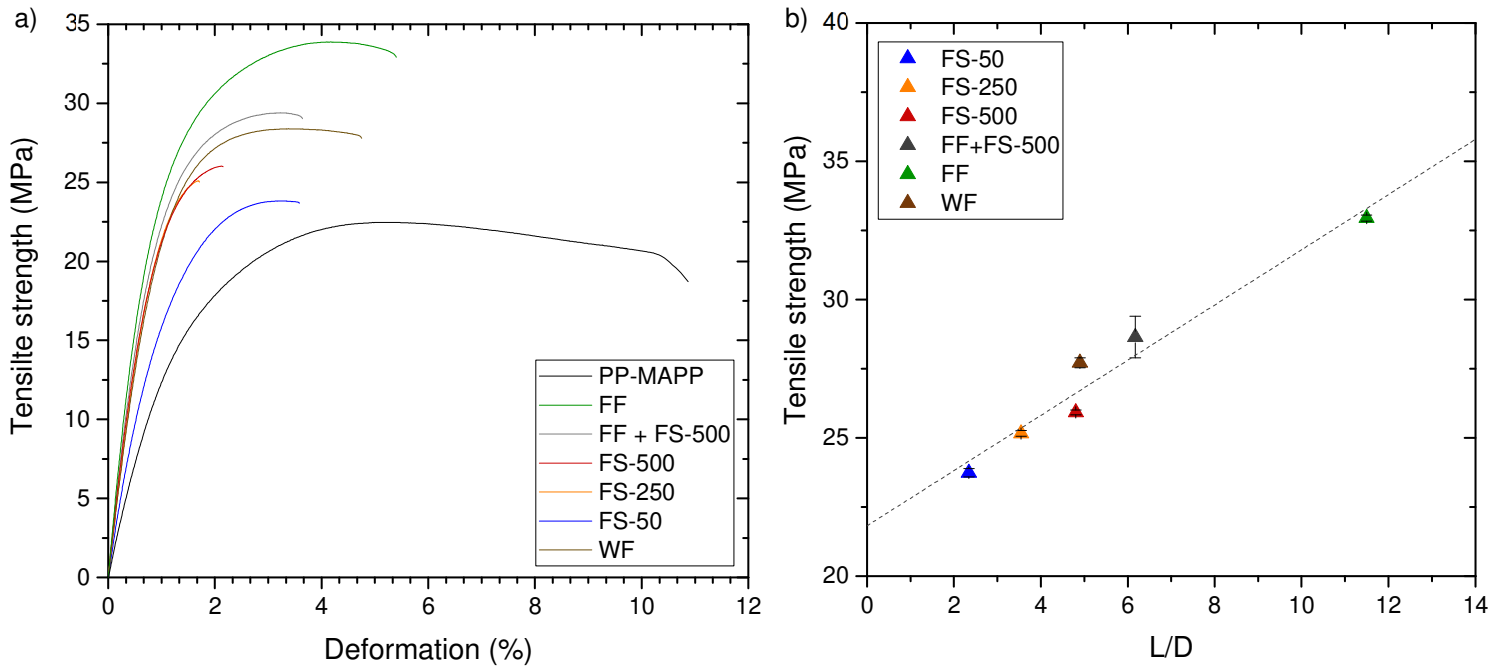


Figure 8. a) Typical tensile stress and deformation behaviour of 30%-wt reinforced PP-MAPP composites, b) Maximum tensile strength of PP-MAPP reinforced composite as function of reinforcing material aspect ratio.

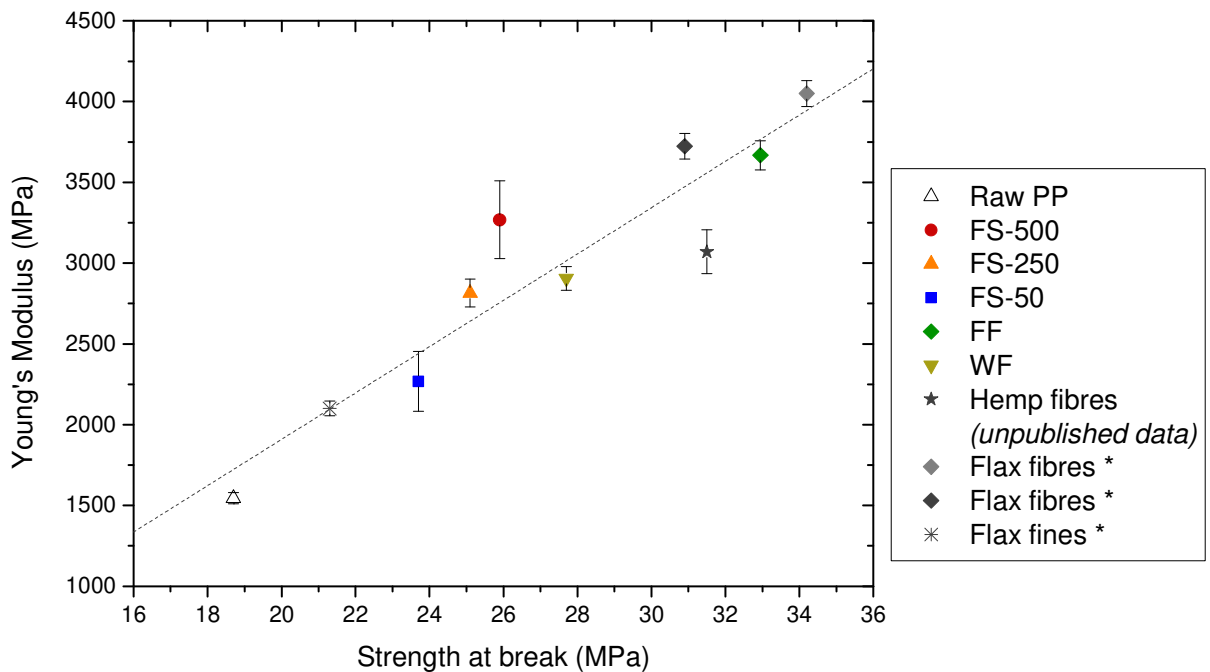


Figure 9. Comparison of mechanical properties provided by different reinforcing materials. For all the batches of this study, both PP-MAPP matrix and extrusion machine are the same. Samples marked with \* are obtained from [40].

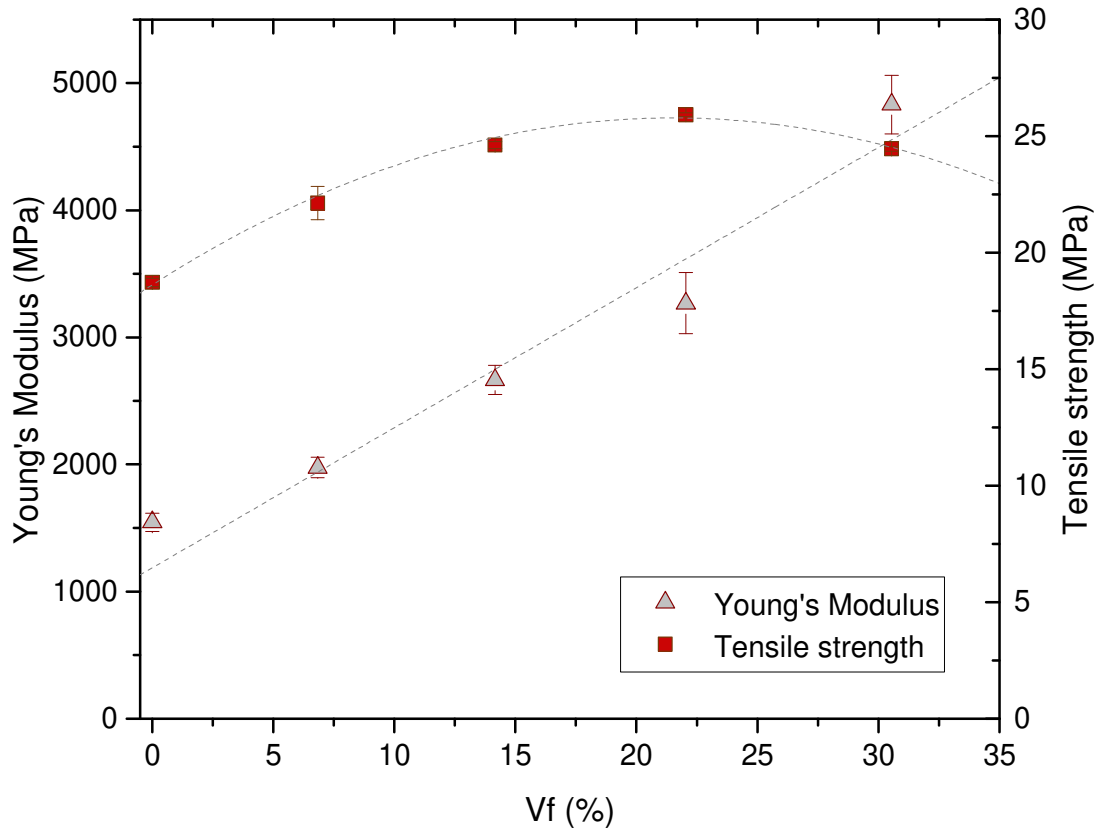


Figure 10. The Young's modulus and maximum tensile strength of FS-500 reinforced composite as function of volume fraction.

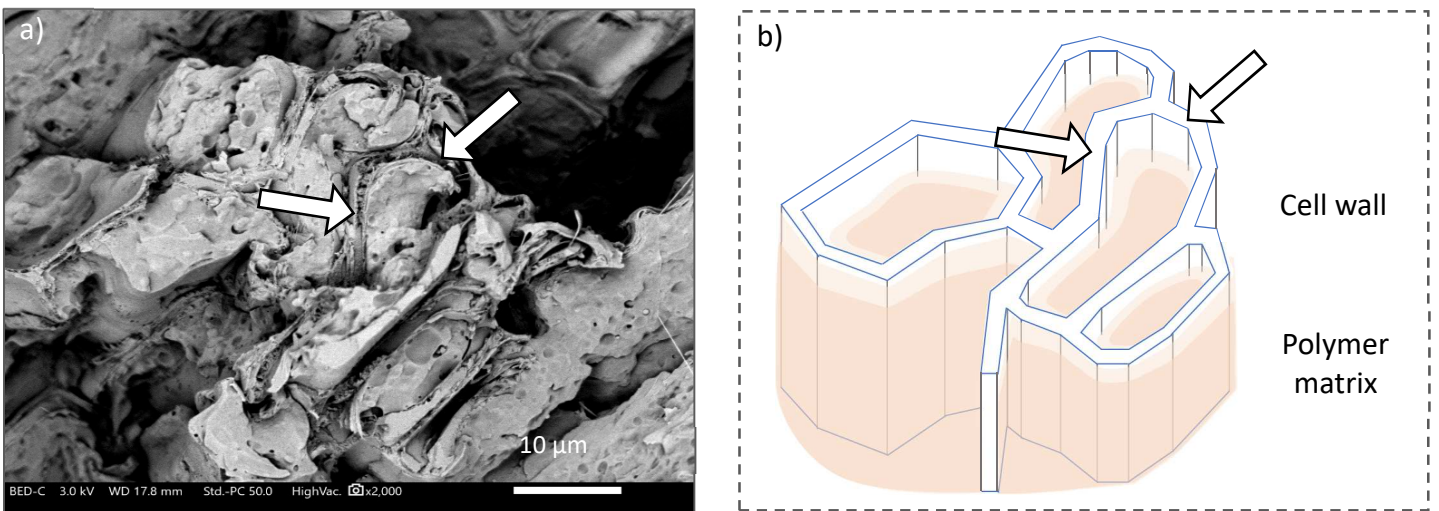


Figure 11. a) SEM observation of the fracture surface of the 30%-wt FS-500 reinforced PP-MAPP composite b) Highlight of a potential matrix penetration in the alveolar structure. Arrows indicate cell-walls.

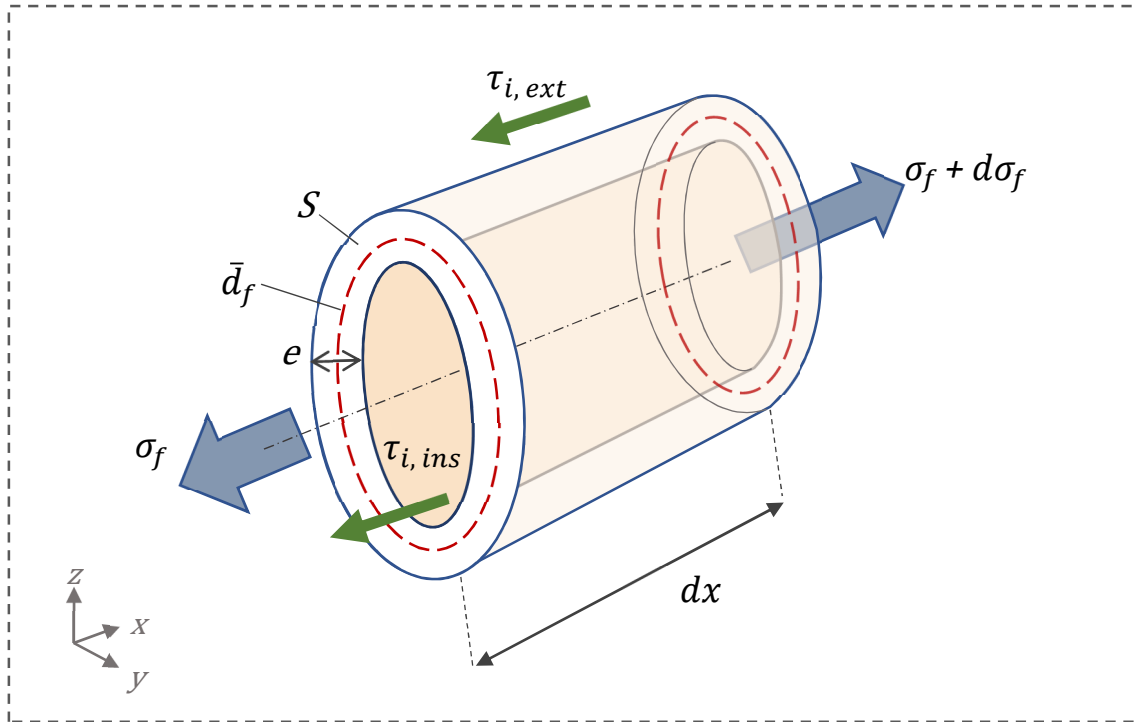


Figure 12. Schematic representation of the mechanical forces applied to a hollow tubular short cell wall structure in a polymer matrix during tensile testing.

Table 1. Reinforcing material samples and corresponding abbreviations.

<b>Sample</b>	<b>Abbreviation</b>	<b>Processing steps</b>
Raw flax shives	R-FS	Obtained from scutching of flax
Flax shives 50	FS-50	Attrition beads milling of R-FS
Flax shives 250	FS-250	Knife milling of R-FS
Flax shives 500	FS-500	Knife milling of R-FS
Flax fibres and flax shives 500	FF + FS-500	50/50-wt mix of FS-500 and FF
Flax fibres	FF	Scutching, hackling and cutting
Wood flour	WF	Fragmentation and sieving

Table 2. Tensile properties of injected composites reinforced with 30%-wt reinforcing materials.

	<b>Young's Modulus</b> (MPa)	<b>Maximum tensile strength</b> (MPa)	<b>Ultimate strain</b> (%)
PP-MAPP	1545 ( $\pm$ 076)	18.7 ( $\pm$ 0.2)	10.9 ( $\pm$ 0.3)
FS-50	2269 ( $\pm$ 185)	23.7 ( $\pm$ 0.2)	3.4 ( $\pm$ 0.4)
FS-250	2815 ( $\pm$ 086)	25.2 ( $\pm$ 0.1)	2.2 ( $\pm$ 0.6)
FS-500	3268 ( $\pm$ 240)	25.9 ( $\pm$ 0.1)	2.3 ( $\pm$ 0.2)
FF + FS-500	3303 ( $\pm$ 083)	28.7 ( $\pm$ 0.8)	3.4 ( $\pm$ 0.7)
FF	3668 ( $\pm$ 090)	33.0 ( $\pm$ 0.1)	5.5 ( $\pm$ 0.2)
WF	2907 ( $\pm$ 073)	27.7 ( $\pm$ 0.2)	4.7 ( $\pm$ 0.1)